EXPERIMENTAL STUDY OF THE INTERACTION BETWEEN ALUMINUM AND HYDROGEN FLUORIDE IN BIOCIDAL EXPLOSIONS

BY

CHRISTOPHER MICHAEL MURZYN

THESIS

Submitted in partial fulfillment of the requirements
for the degree of Master of Science in Mechanical Engineering
in the Graduate College of the
University of Illinois at Urbana-Champaign, 2016

Urbana, Illinois

Advisors:

Professor Nick G. Glumac
Professor Emeritus Herman Krier, Co-Advisor

ABSTRACT

The research presented in this thesis was performed in order to develop a technique for quantitatively measuring the temperature and concentration of hydrogen fluoride (HF) in complex, turbulent flows. These diagnostics were used to investigate the potential suppression of the biocidal species due to aluminum interaction in situ. In the field of counter chemical and biological warfare, explosives are used to evolve spore-killing, and neutralizing agents. Current efforts involve collaboration between experimental and computational laboratories to develop thermochemical models for the biocidal environment. Experiments were conducted to make time resolved, optical measurements that assess the degree of chemical non-equilibrium in these events. From the data collected, the amount of HF generated and rate of equilibration in the biocidal environment was able to be determined.

Two different types of experiments were conducted. The initial set of experiments was designed to closely replicate the detonation of a counter weapon of mass destruction (C-WMD) armament. These tests involved the use of high explosives coupled to solid state halogen fuels. The second thrust area was to create an explosion that replicated the kinetics of the post C-WMD detonation, but simplified the environment to allow higher quality measurements. The simplified explosions used gas phase halogen fuel (1,1-difluoroethane) diffused into a propane/air explosion with pneumatically injected powdered particulates. The results showed that neither the presence of aluminum, nor alumina, suppressed the HF population in the first second of the explosion. The data suggested that if the injected aluminum ignites, it preserves higher concentrations at lower temperatures.

for my sister, Katie

ACKNOWLEDGMENTS

Many of my friends, family, colleagues, and professors deserve to have their name on this page. It would be impossible to thank them all by name, but I am where I am today because of the support and influence from all of them.

Working in this research group has afforded me the opportunity to learn from so many graduate students spanning many years. Starting with Michael Clemenson, Joe Kalman, David Allen, and Lance Kingston. They taught me the skills that it takes to be an experimentalist, and inspired me to work hard. Jeff Shen, Matthew Fitzgerald, Stacy Guo, Jose Guadarrama, and Chee Haw Chan helped push me through the last two years. When classes and work were hard, they were there for me as friends and coworkers.

I am hard-pressed to find words that adequately convey my gratitude towards my thesis advisor, Professor Nick Glumac. Working under his supervision for the past four years exposed me to an unparalleled type of education. I will forever be grateful for all he has done for me as a student and as a scientist.

This research was supported by the Defense Threat Reduction Agency (DTRA), under contract HDTRA1-14-1-0033 .

TABLE OF CONTENTS

CHAPTER 1: INTRODUCTION

1.1. Motivation

"Weapons of mass destruction (WMD) are chemical, biological, radiological, or nuclear (CBRN) weapons or devices capable of a high order of destruction and/or causing mass casualties." The United States' Joint Chiefs of Staff, has identified the need to plan, prepare for, and counter the use of weapons of mass destruction by actors of concern [1]. The Defense Threat Reduction Agency (DTRA) is seeking effective strategies to eliminate collateral effects from the release of a WMD environment. Specifically, Thrust Area 4 – Science to Defeat WMD, is directed at investigating energetic materials with the capability to elevate explosion temperatures, and evolve halogen-containing agent defeat chemicals [2].

One of the most prevalent biocidal chemical species for countering weapons of mass destruction (C-WMD) is hydrogen fluoride (HF). Hydrogen fluoride will combine with water to make hydrofluoric acid which has well documented and studied biocidal effectiveness. Chapman et. al. at the Naval Air Warfare Center in China Lake showed that an N,N-difluoramine explosives, HFNX, cause $\gtrsim 9$ $\log_{10}$ reductions in anthrax surrogate spores when exposed to the explosive products for greater than 5 seconds [3].

The effectiveness of a C-WMD platform is directly related to the amount of halogenated material that obtains a biocidal form and how long it remains that way. Modeling the species concentrations in a post detonation flow is a very difficult task. Much of the current analysis hinges on the thermochemical equilibrium predicted by programs like CHEETAH. The pitfall of

using equilibrium predictions is that post detonation environments are highly turbulent and inherently non-equilibrated. The rate at which conditions converge to equilibrium is unknown. To enable predictive modeling of the biocidal environment, experimental data are crucial to understanding the interaction of fluid mechanics, thermodynamics, and chemical kinetics in the flow following an explosion.

1.2. Previous Work

The field of bio defeat material interaction is fairly nascent. More extensive research has been done investigating material synthesis for developing reactive materials (RM's) that generate known biocides. For example, Zachariah at University of Maryland investigated Aluminum and Diiodine Pentoxide (I_2O_5) for generating molecular iodine as the agent defeat species [4]. Allen, and Glumac from the University of Illinois at Urbana-Champaign also investigated combustion of mechanically alloyed Al-I_2 in a heterogeneous shock tube for its same potential [5].

In contrast to a thermochemical defeat mechanism, there has also been substantial work done to develop advanced RM's capable of thermally disabling biological weapons [6]. Many RM's are mixtures of metals and metal oxides (thermite), or simply two different metals (intermetallic). In addition to fueling thermitic and intermetallic RM's, metals are common additive in many defense platforms purely for their prolific thermobaric capability. The boosts in temperature and overpressure have spore killing benefits of their own. Shock tube and constant volume explosion (CVE) studies have shown the potential this type of neutralization [7, 8]. The limitation of this approach is that any surviving spore colonies would be explosively dispersed which has the potential for collateral damage.

1.3. Project Scope

There is some knowledge for which atomic and molecular species have agent defeat potential, as well as how one can generate them. But there is a notable lack of experimental data about the durability of these species in an explosive environment. To fill this gap, species interactions need to be observed in situ, so scientists can predictively model their behavior.

The specific chemical reaction of interest in this study is that of aluminum and hydrogen fluoride, shown in equation 1. This is a very simplified expression of the reaction that only holds true under certain conditions. In the context of an explosion, the environment will span a very wide range of temperatures and pressures which necessitates very intricate chemical models that remain accurate in all conditions.

$$HF + \frac{1}{3}Al + \frac{1}{4}O_2 \rightarrow \frac{1}{3}AlF_3 + \frac{1}{2}H_2O \quad [1]$$

Chapter 2: *Equilibrium Simulation and Charge Chemistry Design* presents more detailed discussion of the chemical equilibrium, but the problem being addressed, is that thermochemical codes predict aluminum will form aluminum fluoride (AlF_3), instead of alumina (Al_2O_3) at lower temperatures. If the kinetics progress rapidly towards equilibrium, the aluminum will scavenge fluorine away from HF and reduce the spore-killing effectiveness of the C-WMD device. In a biocidal explosion, the presence of agent-defeat chemicals may continue to remain active much longer after the explosion than the temperature or overpressure can. That is provided that they are not consumed or dissipated by other chemical processes. If the

kinetics are sufficiently slow, modeling the biocidal environment using equilibrium models will dramatically underestimate the HF yield from an RM.

CHAPTER 2: EQUILIBRIUM SIMULATION AND CHARGE CHEMISTRY

2.1. Synopsis

This study combined two separate, but collaborative experimental efforts. One effort was to replicate the practical environment in the biocidal explosion, and the other was to simplify the explosive environment and highlight the thermodynamics of interest. For the practical environment tests, high explosives were coupled with solid phase reactive materials and detonated in a constant volume explosion. For the basic science simplification, gas phase fuel/oxidizer mixtures were burned in the presence of solid phase particle suspensions. The same diagnostic equipment was used for both experimental matrices and is detailed in chapter 3.

For both the practical, and simplified experiments, extensive equilibrium modeling was done under the supervision of Dr. Glumac using the Department of Defense thermochemical code, CHEETAH 7. For both test matrices, a baseline chemistry was established that would generate observable quantities of hydrogen fluoride. From that baseline, different aluminum containing molecules were added to the mixture to highlight the reactions progression toward lower enthalpy states predicted by equilibrium. These are shown in

Table 1 as test cases. The mass of each aluminum containing additive was based on the number of moles of elemental aluminum required to completely suppress the amount of hydrogen fluoride produced by the halogen fuel in the article. Equilibrium calculations show the formation of aluminum fluoride over alumina, which is why we chose to compare these two

additives in our system. According to the chemistry, the AlF_3 would not suppress any HF at low temperatures because the aluminum atoms were added with all of the fluorine needed to form AlF_3.

In comparison, the alumina should progress towards aluminum fluoride by scavenging the fluorine atoms away from desired HF molecules. This is an accurate representation of the real explosive environment because, from Figure 1 and Figure 3, it is shown that above 1000 K, the system favors alumina. In the context of an aluminized explosion, the kinetics would favor going to solid alumina at high temperatures immediately following the explosion, and from there, progress towards aluminum fluoride as the gases cool to ambient conditions.

2.2. Practical Environment - Explosive Articles

The halogen fuel used in these articles was polyvinylidene fluoride (PVDF). It is a fluoropolymer with chain structure $(C_2H_2F_2)_n$ and was selected as an effective solid state reactant for producing hydrogen fluoride, as it has both the hydrogen and fluorine atoms in the needed 1:1 mole ratio. This compound is sold commercially under the brand name Kynar®. It was purchased in powder format from Sigma-Aldrich. From preliminary tests, the breakdown of the polymer under explosive loading was found to be potentially inconsistent and incomplete. Potassium perchlorate ($KClO_4$) was added to the mixture to assist with polymer decomposition.

The mass of explosive (RDX, PETN) included in simulation was found from the published values for RP-80 detonators [9]. The mass of air in these simulations reflects one standard atmosphere of air in the blast chamber detailed in Chapter 3.

Table 1: Four test cases used in the practical environment explosive tests

	Case 1		Case 2		Case 3		Case 4	
	mass [g]	mass [%]	mass [g]	mass [%]	mass [g]	mass [%]	mass [g]	mass [%]
PVDF	0.075	3.808%	0.075	3.768%	0.075	3.733%	0.075	3.685%
$KClO_4$	0.075	3.808%	0.075	3.768%	0.075	3.733%	0.075	3.685%
RDX	0.123	6.245%	0.123	6.179%	0.123	6.121%	0.123	6.044%
PETN	0.080	4.062%	0.080	4.019%	0.080	3.981%	0.080	3.931%
Air	1.616	82.076%	1.616	81.206%	1.616	80.447%	1.616	79.428%
Al	-	-	0.021	1.060%	-	-	-	-
Al_2O_3	-	-	-	-	0.040	1.986%	-	-
AlF_3	-	-	-	-	-	-	0.066	3.227%
Total	1.969	1.000	1.991	1.000	2.009	1.000	2.035	1.000

Two different types of simulation were carried out in CHEETAH for each case. The first is a constant volume explosion (CVE) that calculates the post detonation species concentrations as well as estimates energy release. The second type was an isochoric variation of temperature which depicts the equilibrium mole fraction across a range of temperatures in each test case.

The output from the CVE simulation was used to develop a Case 1 test where 103 mg of PBXN-9 was added to match the energy contribution of the aluminum in Case 2. This energy normalization was intended to allow observation of HF at the same elevated temperatures resulting from aluminum addition. The thermodynamic isochors shown in Figure 1 and Figure 3 were used to verify that our article chemistry was indeed predicted by CHEETAH to have significant HF suppression in the presence of aluminum as the gases cool towards room temperature.

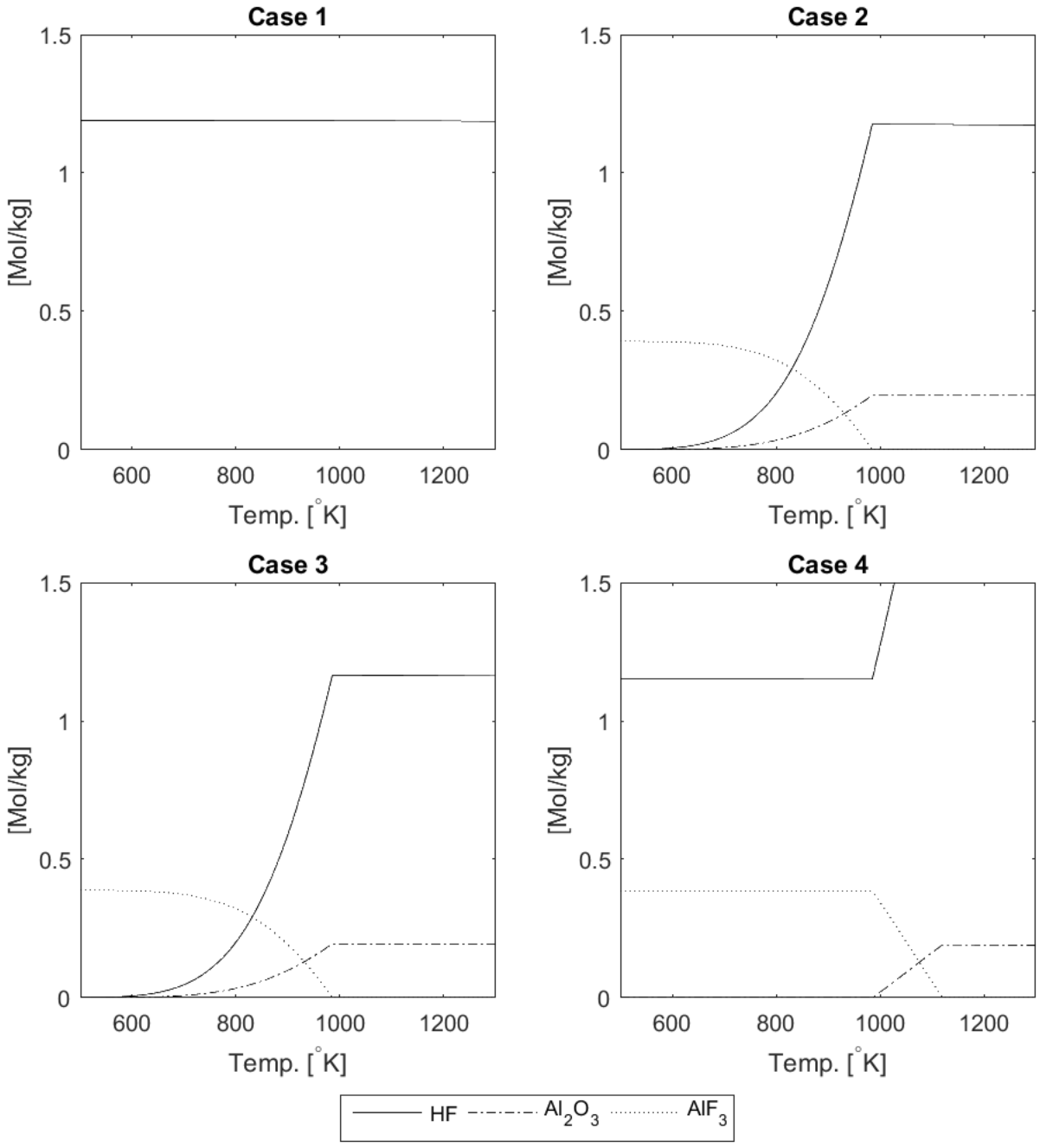

Figure 1: Chemical equilibrium for practical environment test articles as predicted by CHEETAH

In addition to confirming the validity of our test article chemistry, the thermodynamic isochors shown in Figure 1 depict the motivation of this research. Looking at case 2 which theoretically represents the equilibrium behavior of an aluminized C-WMD warhead, it is clear that as the

post explosion gasses cool, aluminum is predicted to suppress the concentration of hydrogen fluoride thereby mitigating the agent defeat capability of the payload. Case 1 represents the baseline combustion of our halogen fuel. The predicted behavior is that the HF will remain at a fixed concentration for the full range of temperatures produced by the explosion.

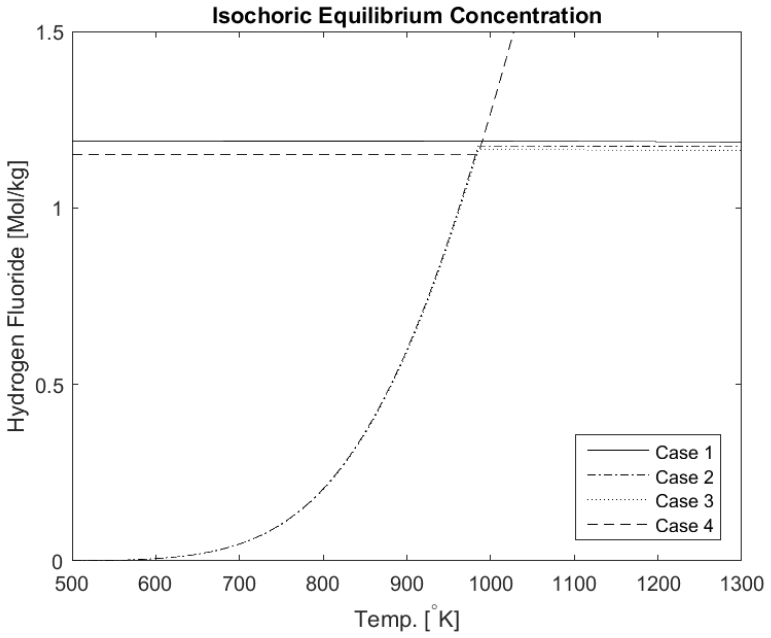

Figure 2: A direct comparison of relative population density of HF in each test case

Figure 2 shows the overlaid concentrations of just the HF species. It is difficult to differentiate on the plot, but Case 2 and Case 3 follow the same asymptotic curve. These are both cases containing aluminum initially, but not in the form of AlF_3. Case 4 that initially has AlF_3, begins to dissociate and rapidly contribute to the HF concentration above 1000 K. The equilibrium obviously predicts that as the explosion cools, the aluminum will rescavenge the fluorine it gave up leaving the low temperature concentration equal to that of Case 1.

2.3. Simplified Environment – Fuel/Air Explosives

In the tests designed to highlight the thermodynamics, the halogen fuel used was 1,1-difluoroethane (DFE). Burning a gas phase reactant helped to ensure more complete molecular breakdown as opposed to the solid phase fuel in the explosive articles. Doing so also reduced the optical depth that arises from testing with high explosives. Equilibrium predictions for a stoichiometric DFE/air explosion suggest substantial hydrogen fluoride production. To create spectral absorption features that would remain sensitive and enable quantification, the baseline (Case 1) mixture was a lean, propane/air explosion with precise quantities of DFE diffused into the reactants. The mass of air used in simulations includes 1 standard atmosphere inside the chamber described in section 3.8, 0.5 psig used to pre-mix the fuel/air in the chamber, and 2.65 psig used to inject powder.

Table 2: Reactant masses simulated in CHEETAH for simplified environment

	Case 1		Case 2		Case 3		Case 4	
	mass [g]	mass [%]	mass [g]	mass [%]	mass [g]	mass [%]	mass [g]	mass [%]
DFE	0.030	3.032%	0.030	3.007%	0.030	2.985%	0.030	2.956%
Propane	0.020	2.024%	0.020	2.007%	0.020	1.993%	0.020	1.973%
Air	0.943	94.945%	0.943	94.167%	0.943	93.486%	0.943	92.568%
Al	-	-	0.008	0.819%	-	-	-	-
Al_2O_3	-	-	-	-	0.016	1.537%	-	-
AlF_3	-	-	-	-	-	-	0.026	2.503%
Total	0.993	1.000	1.001	1.000	1.009	1.000	1.019	1.000

Figure 3 depicts CHEETAH predicted equilibrium behavior for each case. The equilibrium concentrations of this chemical system closely replicates the behavior in the practical explosive case. This is necessary in order to draw conclusions between the two. Note that in Case 4,

equilibrium predicts that the addition of AlF_3 will increase the HF population at higher temperatures, and evidence of this change was clearly observed in our experiments to be discussed later in Chapter 5.

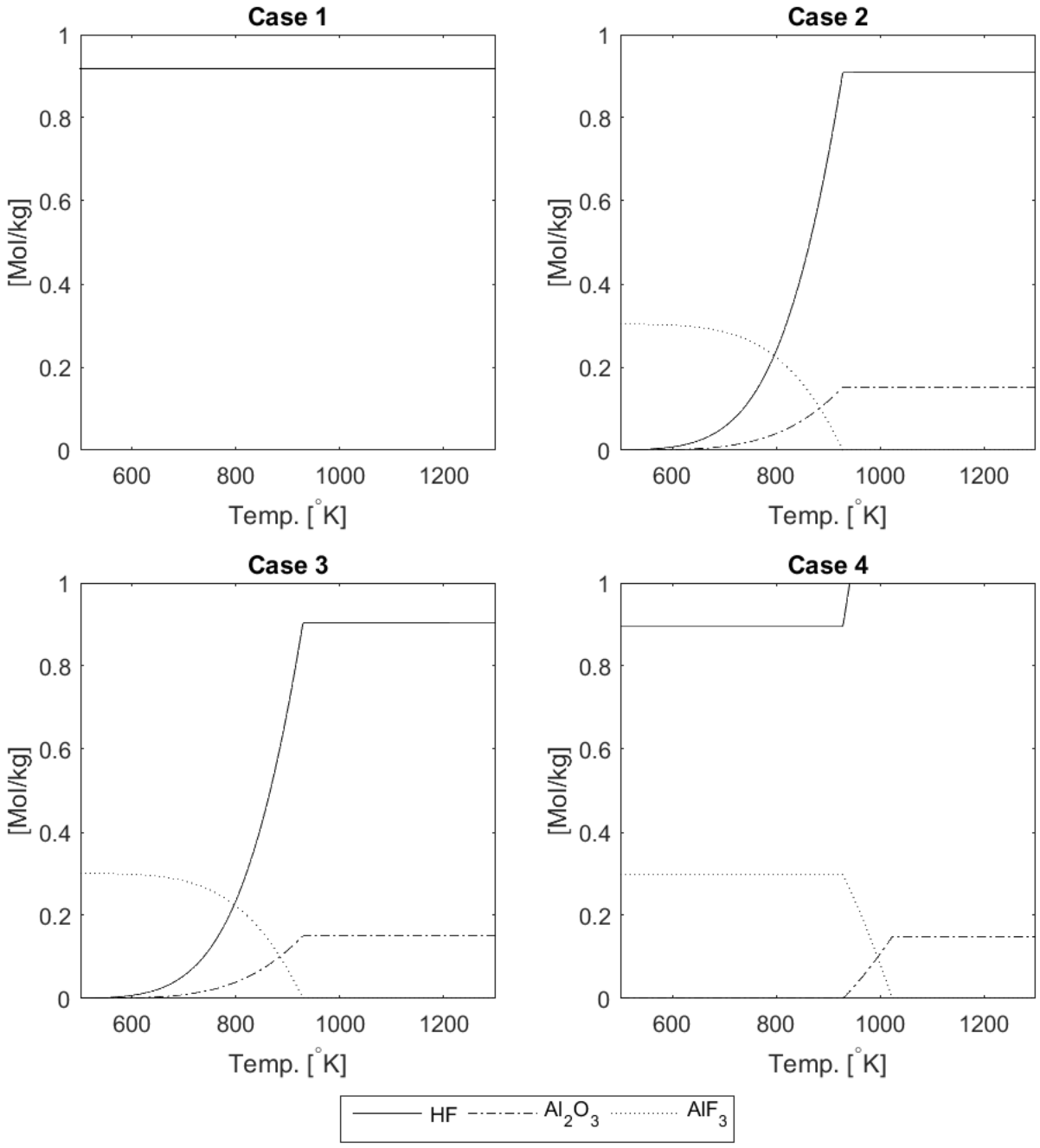

Figure 3: Chemical equilibrium for simplified environment test articles as predicted by CHEETAH

Figure 4 below shows the same type of overlay as described in the practical environment simulation. The predicted degree of suppression for this type of explosion is nearly identical to that of the practical environment cases. CHEETAH predicts an order of magnitude reduction concentration below 700 K.

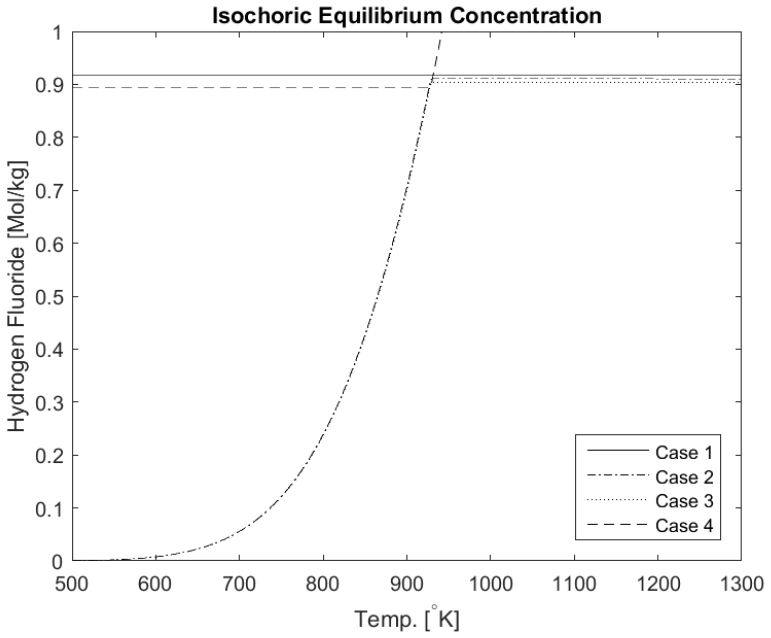

Figure 4: A direct comparison of relative population density of HF in each test case

CHAPTER 3: EXPERIMENTAL METHODS

3.1. Synopsis

Temperature, pressure, and species concentration are the crucial metrics needed to characterize the fluoro-metalic interaction. Both simplified and practical experiments were constant volume explosions. High speed, spectroscopic absorption measurements of the HF overtone band were collected in the near infrared (NIR) wavelengths. The overtone transition is the vibrational transition with $v' - v'' = 2$. In this case, the HF molecules are being excited from the ground state, $v'' = 0$, to the second excited state, $v' = 2$. The lines being observed are the rotational differences in addition to the overtone vibrational change.

More detail is presented in the following sections. However the general idea is that from the spectra, a rotational temperature was calculated. With that temperature, the partition function and HF number density were calculated. With the pressure measurement and the number density, a concentration, in parts per million, was then extracted.

3.2. Spectroscopic Instrumentation

Experiments employed classical absorption spectroscopy measurements in the near infrared spectrum. The spectrograph was a Czery-Turner configuration with a 0.444 meter focal length, and an F/7 aperture. The grating was a gold coated, planar ruled, reflection grating with 1200 gr/mm and a blaze angle of 36.8°. The backlight source was a 400 watt, 36 volt, tungsten-halogen bulb purchased from McMaster Carr. The light from the bulb was collected and collimated by a Ø2 in. calcium fluoride lens with F/1. After passing through the Ø 1.5 in.

windows in the chamber, light was focused onto the entrance slit by a Ø2 in. glass lens with F/4.5.

Our detector for measuring the light was a G9202-512S, indium-gallium-arsenide (InGaAs) linear array being driven by a C7041 detector head and a C7557 controller. All of these components were manufactured by the Hamamatsu Corporation. The InGaAs linear array was 512 pixels with pitch of 25 µm and optical aperture of 250 µm. This setup was capable of frame rates, up to 200 Hz. The simplified matrix tests used a 10 ms rate with 5.897 ms exposure, while the practical tests had a 25 ms rate with 20.897 ms exposure.

3.3. Spectral Line Section

Care was taken in which lines were selected for analysis. The HITRAN database was used to simulate the overtone spectrum at 300 K, 800 K, and 1300 K [10]. This was done to observe line sensitivity to temperature change in the range expected from these explosions. In order to get high quality optical temperature measurements, lines that exhibit dramatic intensity changes are preferred. It was concluded that the R(2), R(3), R(4), and R(5) lines of the first overtone band of HF were excellent candidates for these experiments because between 300 K and 1300 K these lines will demonstrate a relative population inversion as shown in Figure 5. Having large changes in line strength corresponding to smaller changes in temperature made the calculations more robust against measurement error. Additionally, calibrating the spectrograph was straightforward using the 2^{nd} order of a 632.8 nm transition from a helium-neon laser, as it is centered between the R(3) and R(4) transitions.

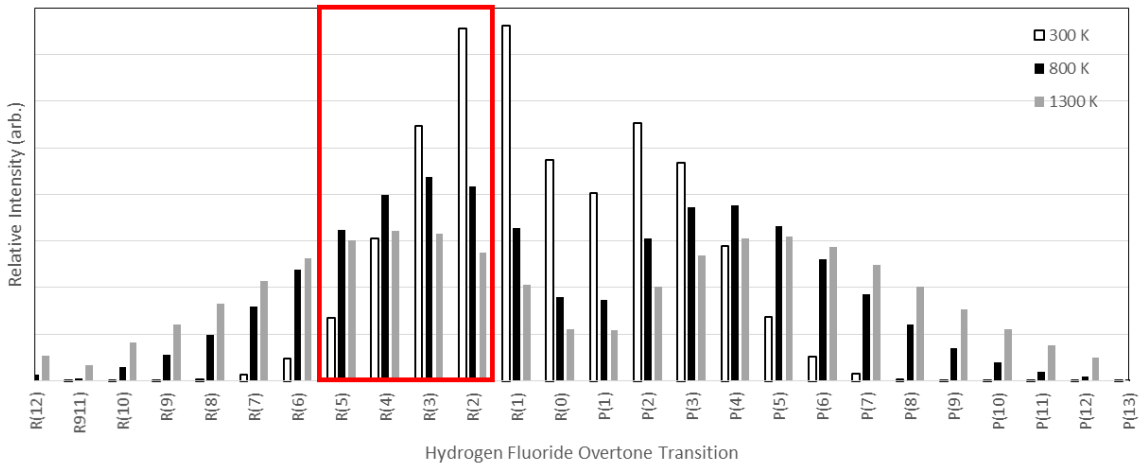

Figure 5: HITRAN simulation of HF overtone temperature dependence

These particular features also contain the benefit of tighter band spacing available in the R branch as depicted in Figure 6 that reflects the accurate spectral distribution at elevated temperatures. The R branch in vibration spectroscopy refers to the lines where $J' = J'' + 1$ [11]. This means that the rotational quantum number of the excited state is one higher than that of the lower state. In the R branch of rovibrational spectra, line spacing decreases with rotational quantum number which can be seen in Figure 6 [12]. Since detectors have a limited size, working with lines in that branch allowed us to fit more features onto the chip. Having more features available for measurement improved the efficacy of our calculations.

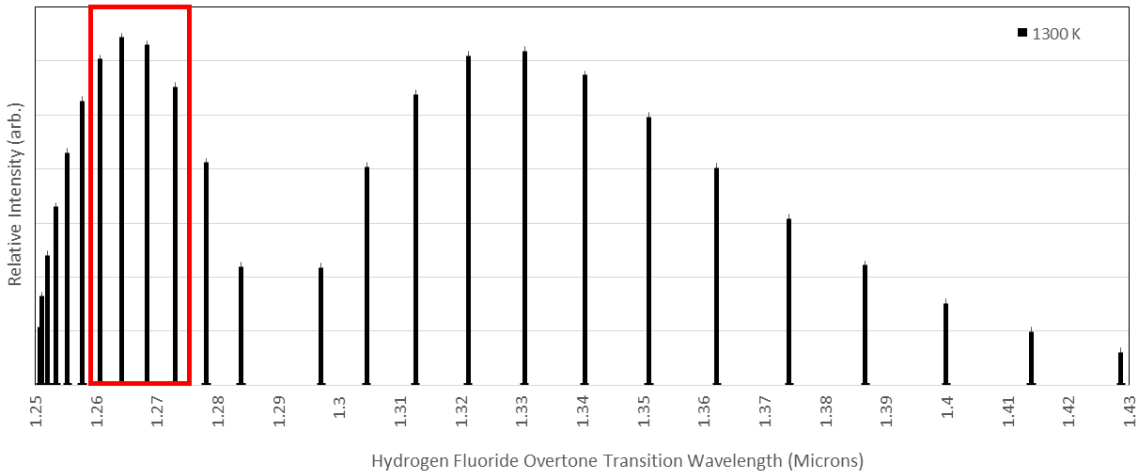

Figure 6: HITRAN simulation of HF overtone band shape and line spacing

3.4. Barometric Instrumentation

To quantify the HF concentration, the chamber pressure is needed. In both blast chambers described in sections 3.7 and 3.8, an Endevco® piezoresistive pressure transducer was used. This was a model 8530B with a rated range of 0 to 50 psia. The signal was amplified through an Endevco® signal conditioner, model 4428A. The probe was mounted in a Delrin® adapter that was compression fit to the exhaust port exiting the top of the chamber. The mounting is shown in Figure 10 and Figure 11. The reason for mounting in Delrin® was to electrically isolate the probe from the electromagnetic pulse generated in the explosions.

Data were collected at the rate of 1 mega-sample per second. This was much higher temporal resolution than the optical collection, so pressures corresponding to the time of each spectrum were matched for calculation. The higher resolution pressure histories allowed for comparison of maximum energy release as well as characteristic comparison of the entire combustion event.

3.5. Equipment Triggering and Diagnostic Networking

Fully characterizing the thermodynamics of the explosion with millisecond scale resolution required a network of cameras, transducers, amplifiers, and oscilloscopes working in tandem, along with the equipment initiating the explosions. In order to capture the greatest amount of data and work around the start delay of the spectroscopic camera, all tests were initiated from the Hamamatsu software running on the DAQ computer controlling the detector head. This enabled us to precisely trigger the explosives and transducer simultaneously as the camera collects its first spectrum.

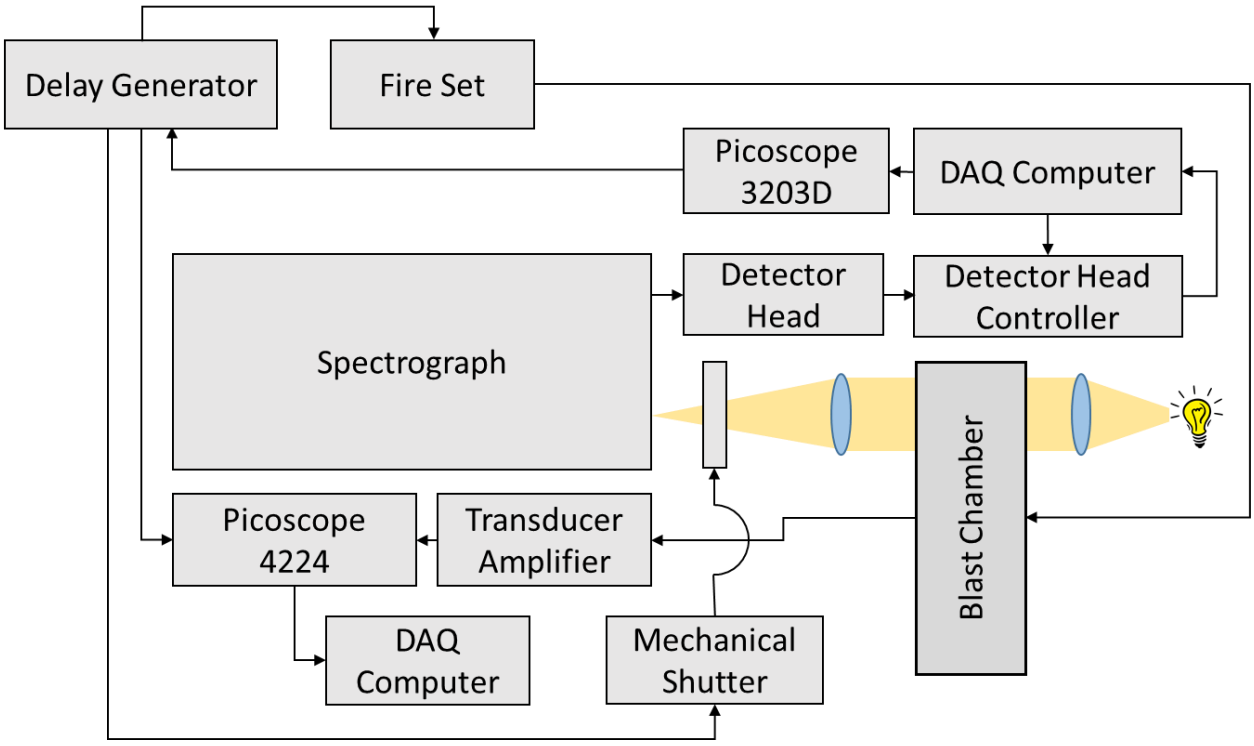

Figure 7: Schematic of diagnostic equipment triggering and data collection

The trigger output from the detector head controller consisted of delta function voltage spikes occurring at the user-set frame rate the camera was collecting at. Initiating the camera from

the internal trigger of the software, the trigger output signal contained additional delta function spikes in between the initial pulses corresponding to frame rate. This trigger output was read by a Pico Technology® 3203D digital oscilloscope. This Picoscope® was chosen explicitly for its ability to take a user specified trigger based on a pulse interval change from camera controller and send an output square wave function that our delay generator recognizes as an external trigger.

The delay generator was central node in the signal train. The start delay of the camera was programmed here to pass before triggering the fire set to detonate the explosives and the 4224 oscilloscope to read voltages from the pressure transducer.

3.6. Practical Environment – Explosive Articles

The practical environment experiments employed the use of an RP-80 exploding bridge wire (EBW) detonator from Teledyne-RISI [9]. It contains a gold bridgewire seated at the bottom of 80 mg of PETN followed by 123 mg of RDX. Figure 8 shows the explosive train configuration. The aluminum cap was removed prior to each test to minimize sources of fluoro-metallic interaction. The remaining detonator apparatus contains a plastic base with the bridge wire and explosive train stacked on top and kept in place with the RP-80's interior brass sleeve. These are referred to as unsealed detonators. The reactive materials being tested were hand mixed powders lightly packed into secondary brass sleeves that were all cut to .6" ±.001 from brass tube stock with 5/16 in. OD and .014 in. wall thickness. Brass was used as an inert material that would provide adequate confinement for our reactive mixtures.

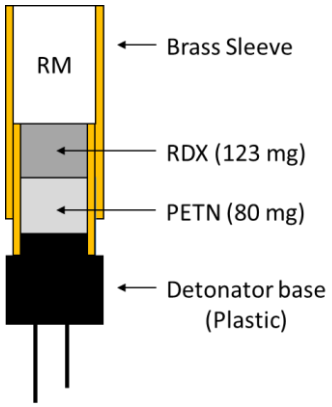

Figure 8: A depiction of the test article configuration used in the practical environment testing

These sleeves were placed on top of the unsealed detonator and wedged in between two anvils. The heavy confinement of the anvils helps to improve the breakdown of reactive powders by prolonging exposure to the high explosive. The top anvil was on a bolt acting as a threaded rod that allowed us to tighten down on the explosive article. The bottom anvil had holes to plum the detonator wires and a counter bore hold the article upright while mounting in the chamber. The mounting of these articles is shown in Figure 9.]

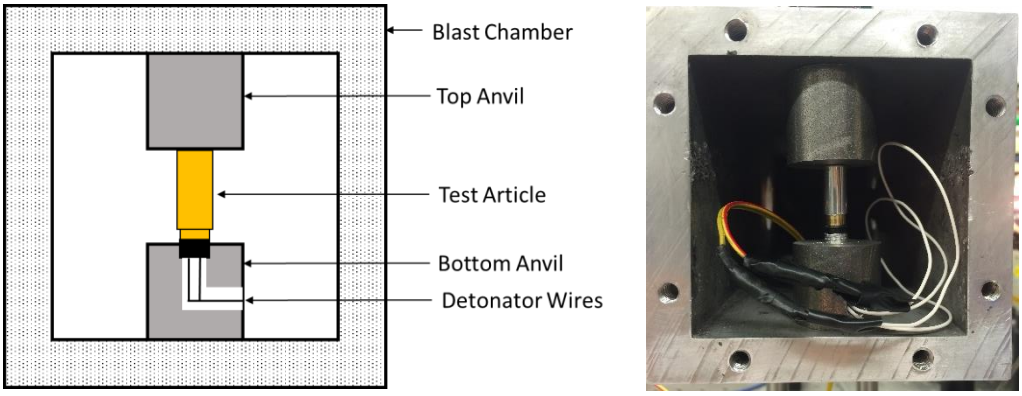

Figure 9: A depiction of explosive article mounting inside the blast chamber

3.7. Practical Environment – Blast Chamber

The blast chamber used for these tests was made from a 4”x4”x10” segment of aluminum square bar with 0.5” wall thickness. It had 1.5” glass windows on the side farthest from the explosive spanning the short dimension of the chamber. This provided a 3.5 inch path length for our absorption to occur. The chamber was fitted with a sodium hydroxide, in line air scrubber that vented into the exhaust system. Additional electrical safeguards were required to dissipate the electromagnetic pulse created during the explosion. The chamber was electrically isolated from the optical table with rubber padding, the transducer fitted with a Delrin adapter, and the pneumatic supply and vent plumbed with nylon hosing. The isolated chamber wall was outfitted with a copper grounding strap leading into the laboratories ground circuit.

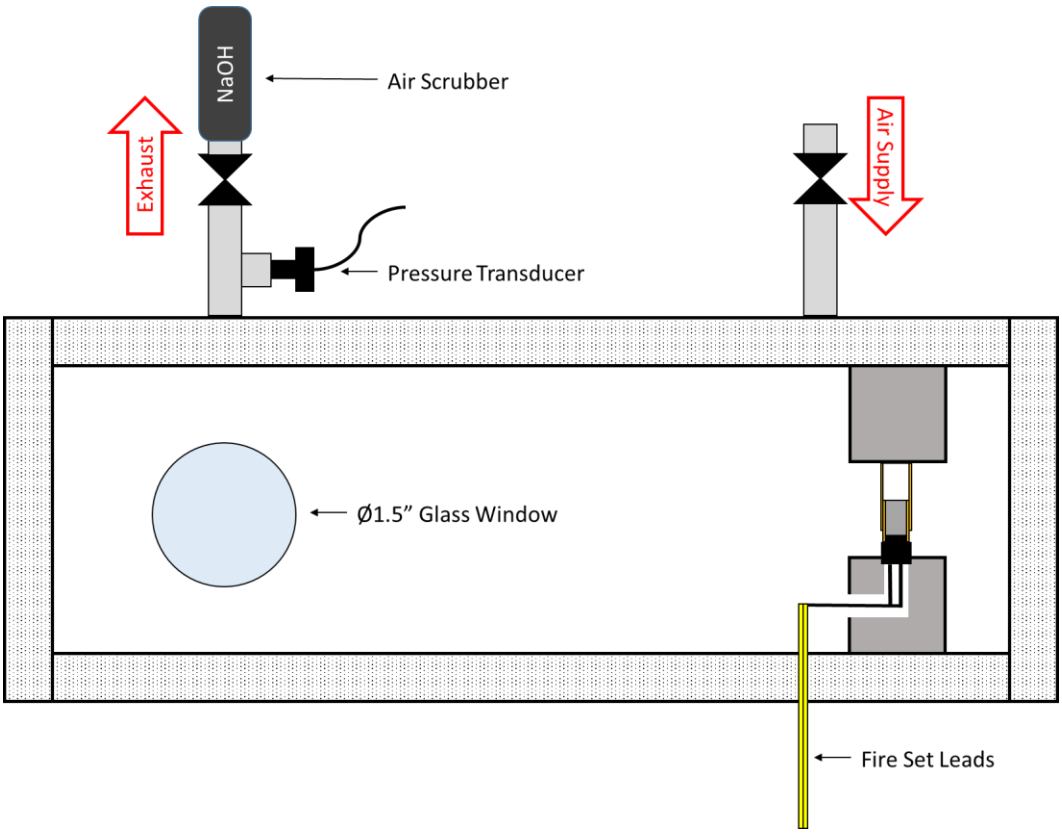

Figure 10: Side on cross section of practical environment blast chamber

3.8. Simplified Environment – Articles and Blast Chamber

Simplifying the thermochemical environment required a slightly more complicated chamber to enable precise control over the environment. This chamber needed to be capable of mixing reactant gases on the order of tenths of a psi, while also supporting the explosive pressures on the order of 50 psi. There was also the additional complexity of injecting solid particulate to mix all of the reactants with very precise timing. Orchestrating the reactants and timing of these explosions was substantially more intricate and is described in section 3.5. The chamber for these tests was a 4" x 4" x 5" aluminum block with a 3" diameter hole bored through the center

along the 5” axis. The interior of this chamber is then cylindrical, with holes on opposite walls providing 2” diameter windows for optical access.

The powders being tested in each explosion were pre-loaded into the particle injector. Following that, precise amounts of DFE/Propane/Air were premixed in the internal volume of the chamber. Controlling the FAE environment we injected into helped to create very consistent explosive events. The chamber is represented in Figure 11.

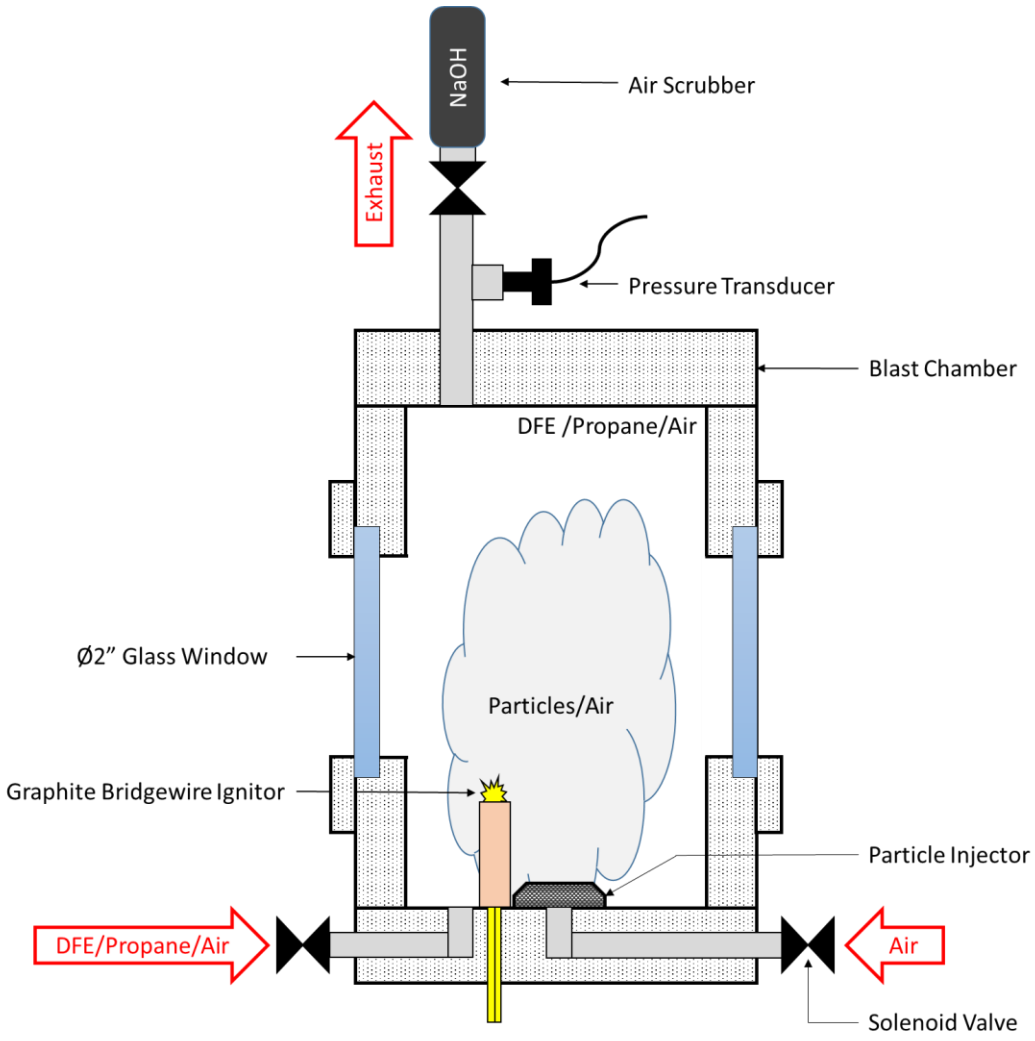

Figure 11: Side on cross section of simplified environment blast chamber

The particle injector was controlled with a solenoid valve and driven with shop air. The solenoid valve was opened and closed with the signal from our delay generator which enabled control over the injection timing relative to all other events. A 10 ms injection was used in all tests. The timing was set so that the powder was injected in the 10 ms immediately preceding ignition. Following the particle injection, a 4 kV discharge across a graphite bridge wire ignited the FAE.

CHAPTER 4: DATA REDUCTION AND CALCULATIONS

4.1. Raw Data Preparation

Data processing and was carried out using MATLAB ®. Readouts from the Hamamatsu software consisted of a .txt file with a header containing information about the detector head and controller. To process the raw intensities, the header was removed leaving only the columns containing intensity values for each spectrum. Once the matrix of values was read into MATLAB®, the average intensity of each image was calculated. Using those averages, saturated spectra were deemed pre-trigger, and removed from the data. The first unsaturated spectrum was labeled the first image and assigned a time corresponding to the length of one exposure value.

4.2. Programmatic Background Correction and Fitting of Raw Spectra

With proper alignment of our optical system, there was a significant presence of etaloning in the spectra collected. Etaloning occurs when light is reflected between two parallel surfaces. This can occur in the glass sheet that sits directly on top of the InGaAs detector. In the spectral domain, etaloning manifests as the repeated high frequency and constant magnitude background oscillation shown in Figure 12. At later test times, and in certain cases with weaker absorption features, the etaloning was on the same order of magnitude of the R(5) spectral line and therefore obfuscated this feature. A sample spectrum of the selected HF lines from a simplified environment test containing aluminum (Test 19) is shown in Figure 12.

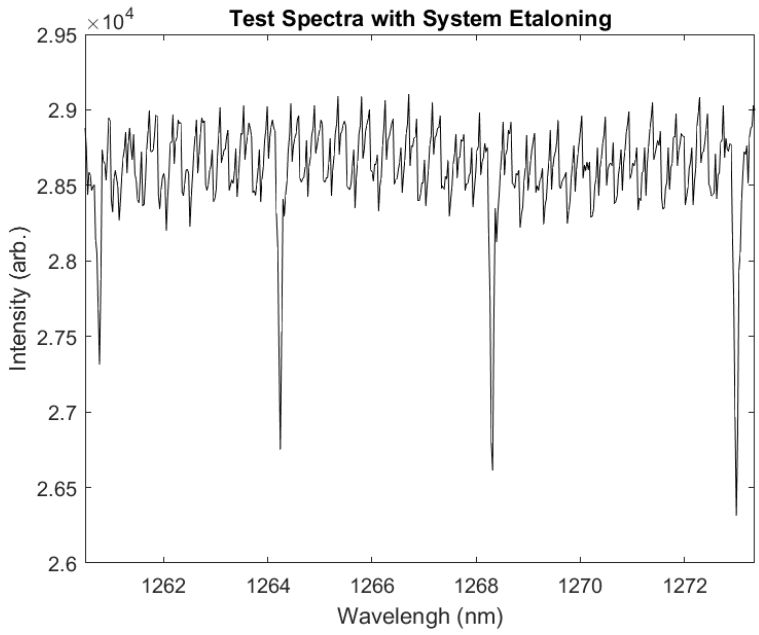

Figure 12: Sample spectrum containing chip etaloning and hydrogen fluoride spectral signature

To enable more accurate measurement of equivalent widths, a novel background fitting procedure was created to reduce the raw data. The fit required three sets of spectra. The first set was a set of 100 sequential spectra spaced at the set frame rate taken prior to the test with a neutral density filter (ND1) in place. The second set was the 100 spectra collected during the explosion. The third set was a 100 shot measurement taken after the test is over.

The fitting algorithm averaged the 100 shots from sets 1 and 3. It then created a mean-normalized reference spectrum by dividing set 1 by the average value of all pixels. From there, each spectrum in set 2 was divided by the mean normalized reference spectrum to help eliminate pixel to pixel noise. This created the mean normalized test spectrum shown in Figure 13.

The third set of data was required to help remove etaloning present in our optical system. Post-test spectra did not contain spectral features of hydrogen fluoride, so when divided by the mean normalized reference, the resulting spectra only contained the undesired etaloning. This spectrum is referred to as the mean normalized post-test spectrum in Figure 13. Individual spectra in set 2, and the 100 shot average of set 3, were spline fit with a high frequency filter to allow the etaloned spectra to be mapped onto the test spectrum. The spline fit curves are represented as solid red lines in Figure 13. This provided a background to divide our raw data from that included the etaloning in the chip. The magnitude of the etaloning in the background image was scaled to match that of the etaloning visible in the each test spectrum. A small section of the test spectrum's background and the algorithm's resulting fit is shown in Figure 13. This spectrum is from a simplified environment test. The same background fitting algorithm was used in both the practical and simplified environment tests, with the exception of using a smaller span parameter in the smoothing of the explosive tests. The reduced span was found empirically to provide better background fits for those tests.

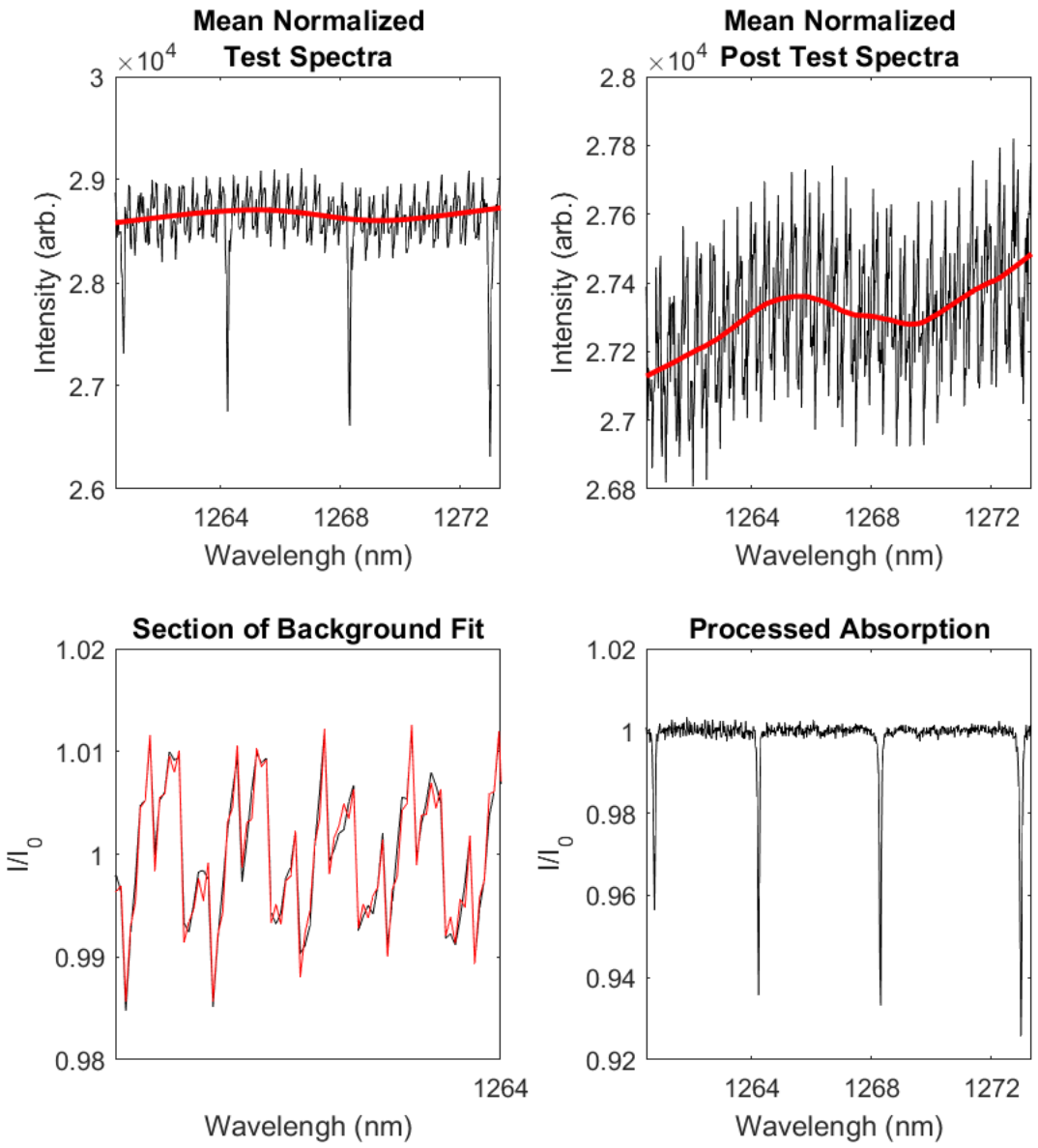

Figure 13: Graphical representation of spline-fit background correction for etaloning

The reduced optical depth in the simplified environment was one of the driving reasons for designing that matrix because it produced much higher resolution spectra that we could measure more accurately. The combination of high fidelity background fitting with the optically

thin explosion yielded dramatically higher resolution spectra with resolution better than 0.2%. This is shown later in Figure 23.

4.3. Equivalent Width Correction for Non-Linear Curve of Growth

Absorption depths recorded in these experiments were substantial enough to slightly depart the linear regime of hydrogen fluoride's curve of growth. To address this we implemented a correction function. This algorithm was originally written by Dr. Nick Glumac and converts equivalent widths to column number densities by matching measured widths to an optical depth, and then calculating the associated width if the number density were in the linear regime. Corrections were made by fitting the experimental peaks with a pseudo-Voigt profile. Calculations were executed using known molecular properties of hydrogen fluoride, a collisional diameter of 3Å [13], published transition constants [14], and measured pressures. Initial inputs for temperature were made using the spectroscopically calculated temperature from the uncorrected equivalent widths. After appending the widths, system temperatures were recalculated. The effect of these correction terms was more prominent as the molecules cool, and the population relaxes into the R(2) and R(3) lines giving them stronger absorptions and therefore more substantial corrections. Figure 15 shows the corrections for the spectrum in Figure 14 which is a test from the simplified matrix. The features with stronger absorptions required more correction.

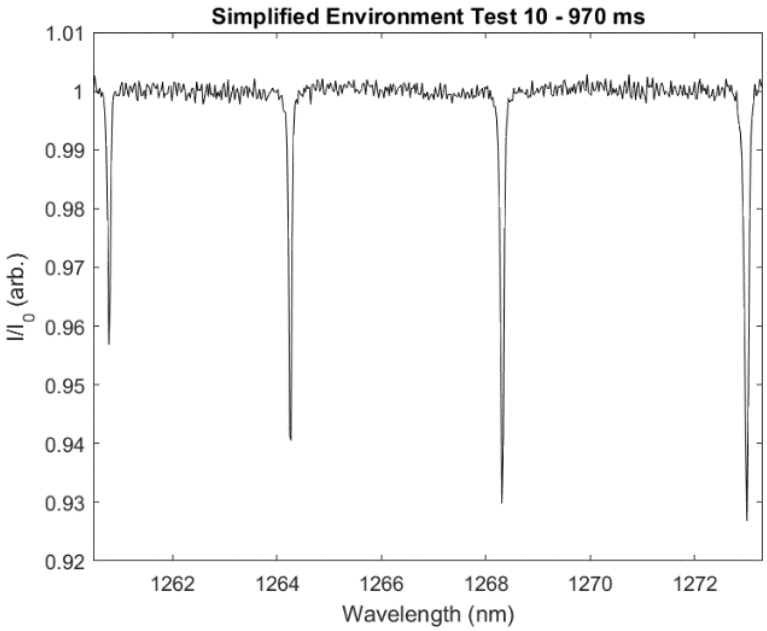

Figure 14: Absorption spectrum from simplified environment test

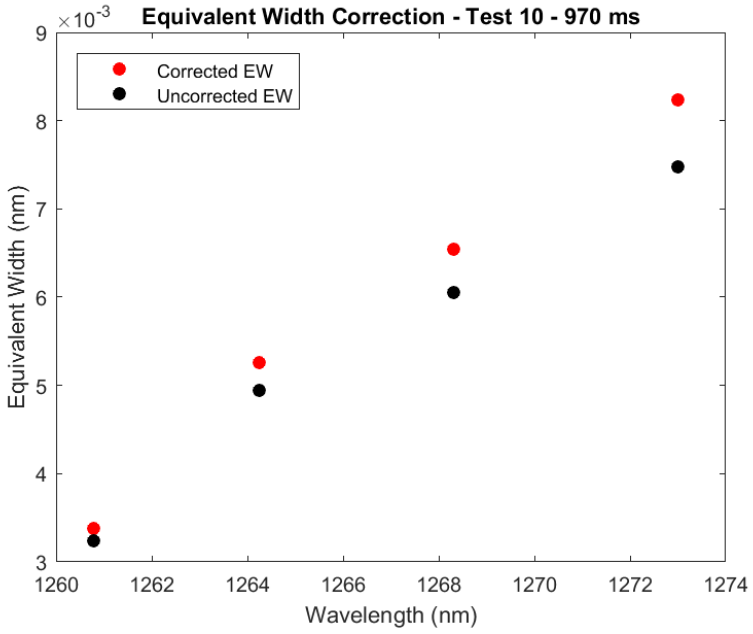

Figure 15: Equivalent width correction corresponding to spectrum in Figure 14

In order to minimize the amount of correction required, and if necessary, make comparisons without correction, iterative tests were conducted to establish baseline chemistry that remained less than 10% absorption depths. Figure 16 shows the peak absorptions of central wavelengths observed over the duration of a simplified environment test (Case 1).

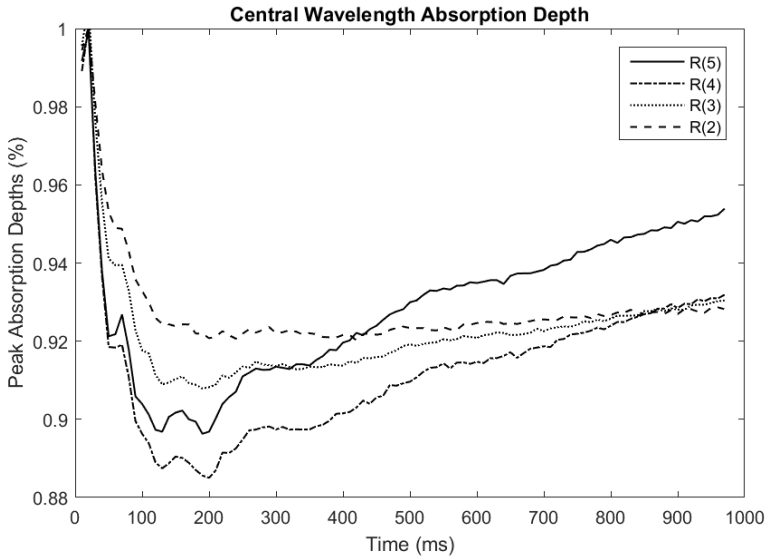

Figure 16: Temporal trace of peak absorption depths from simplified environment baseline test

Figure 17 shows the effect that this correction had on the temperature profile of the explosion. The cases containing AlF_3 required slightly larger corrections due to their stronger absorptions from HF contribution. Those absorptions were typically less than 15%, and remained that high for short durations of the test.

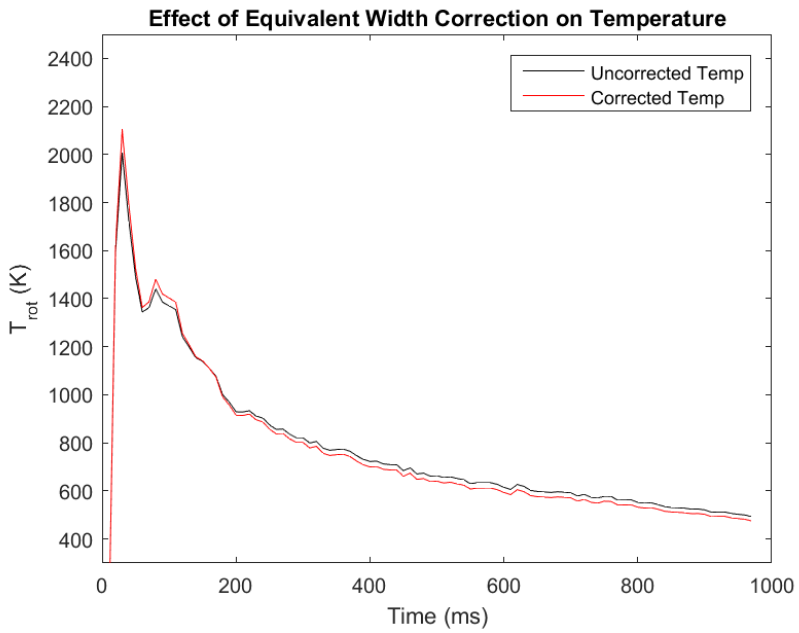

Figure 17: Corrected and uncorrected temperature curves from simplified environment test 10

4.4. Temperature Calculation

Optical temperature measurement from broadband spectroscopy is well known, and documented in the literature. For these experiments, the process detailed in Laurendeau was used [11]. With the equivalent widths obtained using the procedure detailed earlier, Equation 2 can be applied to construct a Boltzmann plot. From the slope of a linear regression the rotational temperature is extracted.

$$\ln\left(\frac{W_{lu}\lambda}{A_{lu}g_l}\right) = \left(\frac{1}{k_B T_{rot}}\right) E_l + \Gamma \qquad [2]$$

It is important to note that in these tests, calculation of temperature and species concentration is only possible at times when measureable hydrogen fluoride features are present. Rotational

temperatures are known to equilibrate rapidly, and therefore these values are a good representation of gas phase temperatures, but the unrepresentative of the solid state particles suspended in the flow. Non-homogenized temperature effects are discussed further in Chapter 5.

4.5. Concentration Calculation

In order to reduce the spectra into quantifiable species concentrations, a number of intermediate calculations were first necessary. In the most reduced form, all of the necessary information is contained in equivalent width, temperature, pressure, and transition constants.

The first step used equivalent widths to obtain lower number density, $n(J'')$ for each line. As mentioned earlier, the Einstein coefficients were obtained from the HITRAN database. The path length, L, was that of our chamber described in Chapter 3. The equivalent widths used were the corrected values.

$$n(J'') = \frac{cW_{lu}}{h\nu_{ul}B_{lu}L} \quad [3]$$

Through lower number density, we calculated a total number density, n corresponding to each line. However in addition to $n(J'')$, total number density is also a function of the electronic partition function, Z_{el}, the rovibrational partition function, Z_{RV}, the electronic degeneracy, $\varphi(2s+1)$, the rotational degeneracy, $(2J''+1)$, the associated lower state rotational energy, $E(J'')$, and the temperature.

$$n_{HF} = \frac{Z_{el} Z_{RV} n(J'')}{\varphi(2s+1)(2J''+1)} exp\left\{\frac{E(J'')}{k_B T}\right\} \quad [4]$$

The temperature used was based on the optically measured and calculated values described in section 4.1. Lower state energies and rotational degeneracies were obtained from the HITRAN database, and confirmed with calculations based on diatomic constants available through NIST [10, 14]. The NIST database also listed the 1st excited electronic state as continuous absorption beginning at 60,600 cm^{-1}. Given the temperatures in these explosions, this energy is sufficiently large to allow the assumption that any excited electronic states were unoccupied and therefore Z_{el} is taken to be unity. The electronic degeneracy was also unity because hydrogen fluoride has $^1\sum^+$ configuration in the X state.

The rovibronic partition function is temperature dependent and therefore was evaluated with the calculated temperature corresponding to each spectrum in the test. Both first and second order correction terms were applied to the rigid-rotor/harmonic oscillator model in order to obtain more accurate values for Z_{RV}. This was done because hydrogen halides are known to experience strong rotation-vibration coupling due to their molecular structure. These corrections are summarized below, with a more explicit derivation available in Laurendeau's text [11].

$$Z_{RV} = Z_{RV}^{\circ} Z_{corr} \quad [5.0]$$

where

$$Z_{RV}^{\circ} = \frac{1}{\sigma}\frac{1}{y(1-e^{-t})} \quad [5.1]$$

$$Z_{corr} = \frac{1}{\sigma}\ 1 + \frac{y}{3} + \frac{y^2}{15} + \frac{2\gamma}{y} + \frac{\delta}{e^t - 1} + \frac{2x^* t}{(e^t - 1)^2} \quad [5.2]$$

The partition function evaluated for each spectrum during the duration of the explosion has a characteristic resemblance to the temperature profile given the dependence. Figure 19 depicts the strong correlation to the temperature profile in Figure 18.

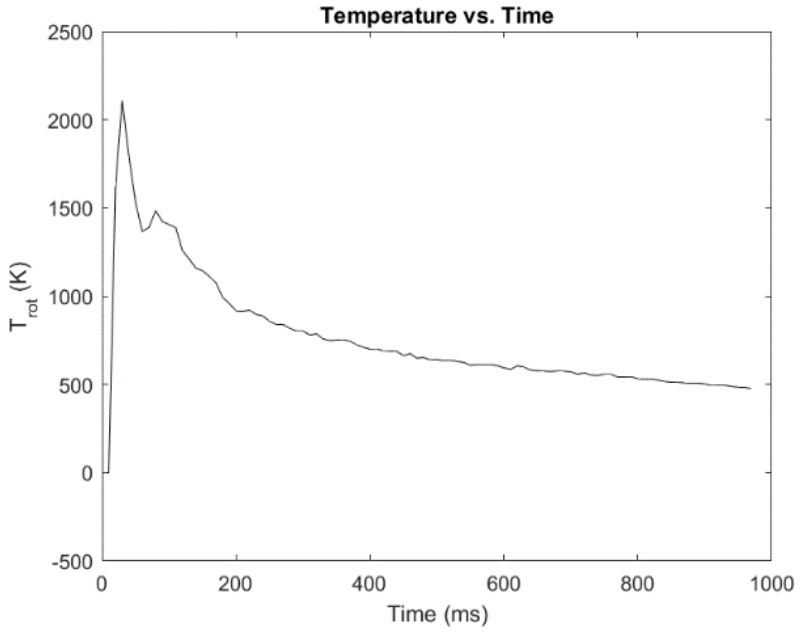

Figure 18: Simplified environment Test 10 temperature history

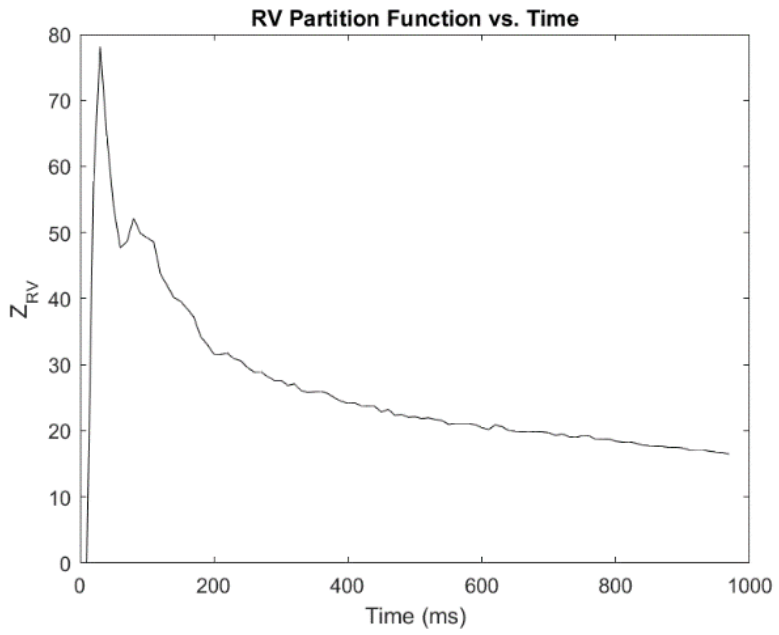

Figure 19: Rovibrational partition function for temperature history shown in

After all intermediate calculations were carried out, the total number density was calculated. The final step taken was to convert total number density into parts per million, which is a more accepted format when discussing agent defeat capability of an explosion because it represents the local population with neutralization potential. Spore survivability is often evaluated in the duration that it can survive a given concentration.

$$n_{chamber} = \frac{P}{k_B T} \quad [6]$$

The conversion from total number density to parts per million was fairly trivial, as it only involves normalizing the number of molecules of HF in the chamber at a given time to the total number of gaseous molecules using equation 7. To calculate number density in the chamber we

employed equation 6, the ideal gas law, using the absolute pressure from the transducer, and the calculated temperature from each spectrum. Thus,

$$C_{ppm} = \frac{n_{HF}}{n_{chamber}}(10^6) \quad [7]$$

CHAPTER 5: RESULTS AND CONCLUSIONS

5.1. Early Time Hydrogen Fluoride Emission

In both the practical and simplified explosions, one test was conducted to address the possibility of early time emission. This was done by performing one test identical to other tests in each matrix, with the exception that the tungsten-halogen backlight was turned off.

In the practical environment, an aluminized high explosive (Case 2) was fired because the elevated temperature from metal combustion exacerbates the emissive behavior. In the simplified environment a baseline (Case 1) shot was fired.

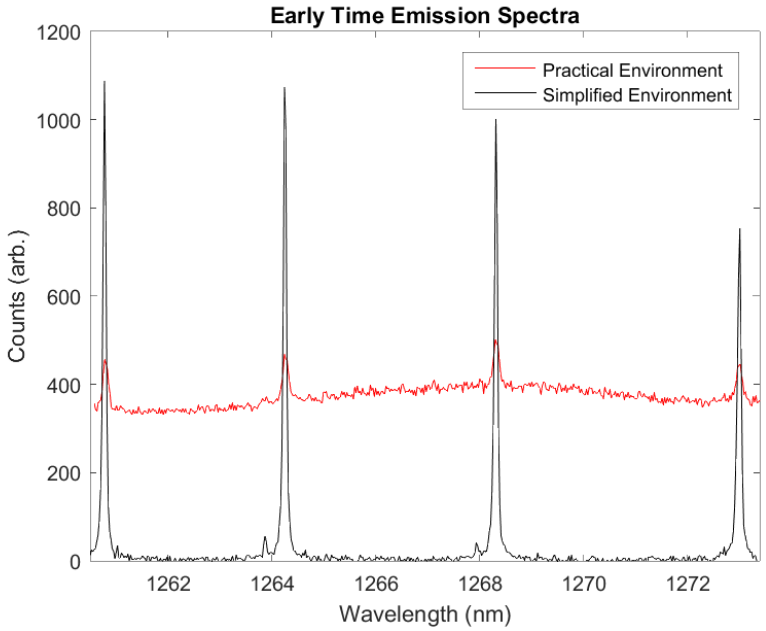

Figure 20: Emission spectra collected to address degree of early time emissive contributions

From Figure 20 it is clear that early time emissive behavior was present. The practical environment contained a notable thermal continuum in addition to small HF artifacts. The

thermal continuum is likely due to incandescent particulate in the high explosive debris. In the simplified environment where the FAE is extremely optically thin, the emission only contains spectral features of HF.

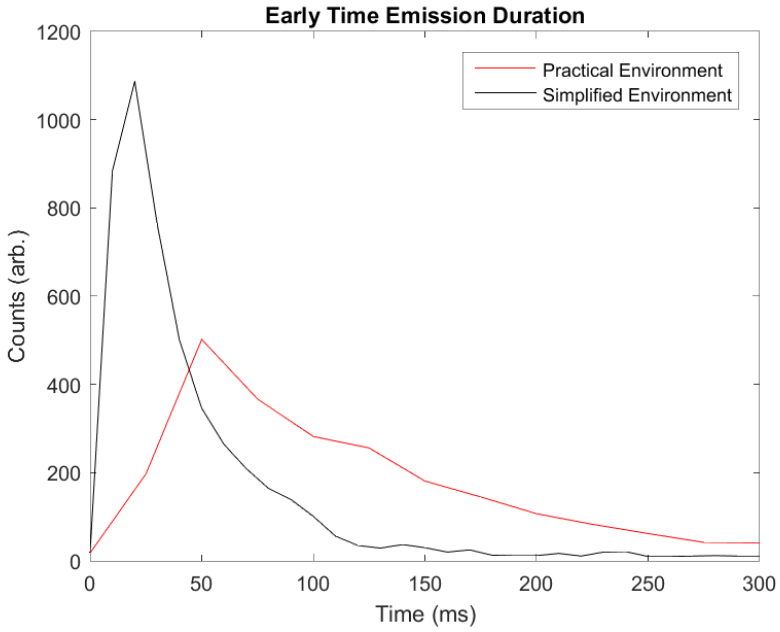

Figure 21: Duration of emissive contributions from both test types

The duration of the emissive contributions is shown in Figure 21. The exact time of the start for these tests was unknown, because there was no reduction in optical depth, or rise from a shutter opening to indicate the exact start of the event. For that reason the beginning of the rise in each shot was said to be time zero.

5.2. Optical Depth

Comparing the optical depth of the two different explosions illustrates the clear advantages of the simplified, academic explosions. The simplified environment averaged 84.67% transmission compared to 2.75% for the practical explosions. To obtain sufficient signal on our detector, a

longer exposure and therefore slower frame rate was required for the practical environment. This is reflected in the longer duration curve in Figure 22. The transmission curves shown were both taken from AlF_3 tests. (Practical – Test 4, Simplified – Test 7)

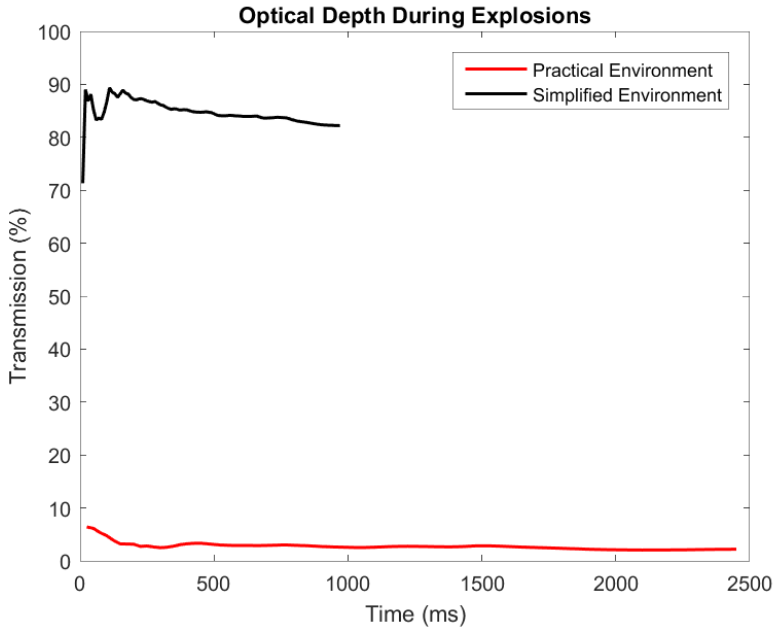

Figure 22: Optical depth measurements from both test types

In addition to measuring at higher frame rates, the resolution in the optically thin tests was on the order of 0.1% compared to 1% in the thick events. The practical environment testing demonstrates our technique's ability to make time resolved, quantitative measurements in optically thick explosions generated from high explosives. For the purpose of definitively observing molecular differences in composition, the simplified environment is a much more useful tool.

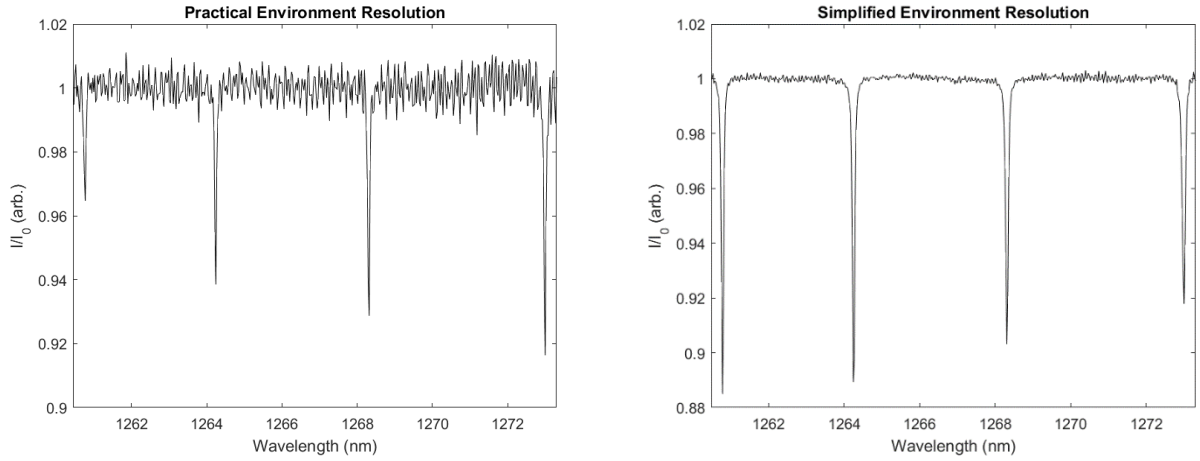

Figure 23: Comparison of practical environment (left) and simplified environment (right) optical depths

5.3. Simplified Environment Test Results

The simplified environment test data will be presented first to establish expected results in order to compare to the practical explosive tests. In total, four baseline, three AlF_3, nine Al_2O_3, and 5 Al tests were conducted in this matrix. In the cases containing alumina, three tests each were conducted at 1x, 2x, and 4x powder loading. The multiplier in the alumina refers to the mass added relative to "1x" being the theoretical amount of alumina required to completely suppress the HF evolved from full conversion of 0.25 psig (30 mg) of DFE in our blast chamber. The mass of air includes 1 standard atmosphere of air in the chamber, 0.5 psig used to flush the fuel lines, and 2.65 psig used in the 10 ms powder injector.

In the case of baseline tests, the injector air was still fired with no powder in the hopper. The powder used in all alumina cases was 300 nm from Alfa Aesar, and the aluminum was 50 nm. The aluminum fluoride used was also purchased from Alfa, with no size grading available. This powder was prepared in a mortar and pestle. Higher powder loadings of alumina were tested

to address differences between mass injected and mass available for catalysis on the surface of solid particles. Some of the results in this section are based on the temporally averaged values for repeated tests. Due to the emissive behavior discussed earlier, only data after 100 ms are compared.

Table 3: Simplified environment test record and masses

Test	Case	DFE ($C_2H_4F_2$)		Propane (C_3H_8)		Air		Powder Additive	
[#]	[#]	[psia]	[g]	[psia]	[g]	[psia]	[g]	[Powder]	[g]
1	1	0.25	0.030	0.25	0.020	17.85	0.943	-	-
2	1	0.25	0.030	0.25	0.020	17.85	0.943	-	-
3	1	0.25	0.030	0.25	0.020	17.85	0.943	-	-
4	1	0.25	0.030	0.25	0.020	17.85	0.943	-	-
5	4 (1x)	0.25	0.030	0.25	0.020	17.85	0.943	AlF_3	0.0262
6	4 (1x)	0.25	0.030	0.25	0.020	17.85	0.943	AlF_3	0.0255
7	4 (1x)	0.25	0.030	0.25	0.020	17.85	0.943	AlF_3	0.0256
8	3 (1x)	0.25	0.030	0.25	0.020	17.85	0.943	Al_2O_3	0.0163
9	3 (1x)	0.25	0.030	0.25	0.020	17.85	0.943	Al_2O_3	0.0153
10	3 (1x)	0.25	0.030	0.25	0.020	17.85	0.943	Al_2O_3	0.0155
11	3 (2x)	0.25	0.030	0.25	0.020	17.85	0.943	Al_2O_3	0.0315
12	3 (2x)	0.25	0.030	0.25	0.020	17.85	0.943	Al_2O_3	0.0303
13	3 (2x)	0.25	0.030	0.25	0.020	17.85	0.943	Al_2O_3	0.0307
14	3 (4x)	0.25	0.030	0.25	0.020	17.85	0.943	Al_2O_3	0.0672
15*	1	0.25	0.030	0.25	0.020	17.85	0.943	-	-
16	3 (4x)	0.25	0.030	0.25	0.020	17.85	0.943	Al_2O_3	0.0663
17	3 (4x)	0.25	0.030	0.25	0.020	17.85	0.943	Al_2O_3	0.0665
18	2 (1x)	0.25	0.030	0.25	0.020	17.85	0.943	Al	0.0082
19	2 (1x)	0.25	0.030	0.25	0.020	17.85	0.943	Al	0.0081
20	2 (1x)	0.25	0.030	0.25	0.020	17.85	0.943	Al	0.0081
21	2 (1x)	0.25	0.030	0.25	0.020	17.85	0.943	Al	0.0082
22	2 (1x)	0.25	0.030	0.25	0.020	17.85	0.943	Al	0.0079

*Baseline test conducted to measure early time HF emission

Figure 24 and Figure 25 present data that verify our baseline and alumina tests experienced very similar temperatures and pressures, which enables direct comparison between different

cases. Looking specifically at the temperature curves, there is evidence of a very slight decrease in temperature which we attributed to heat absorbed by the powder in our explosion.

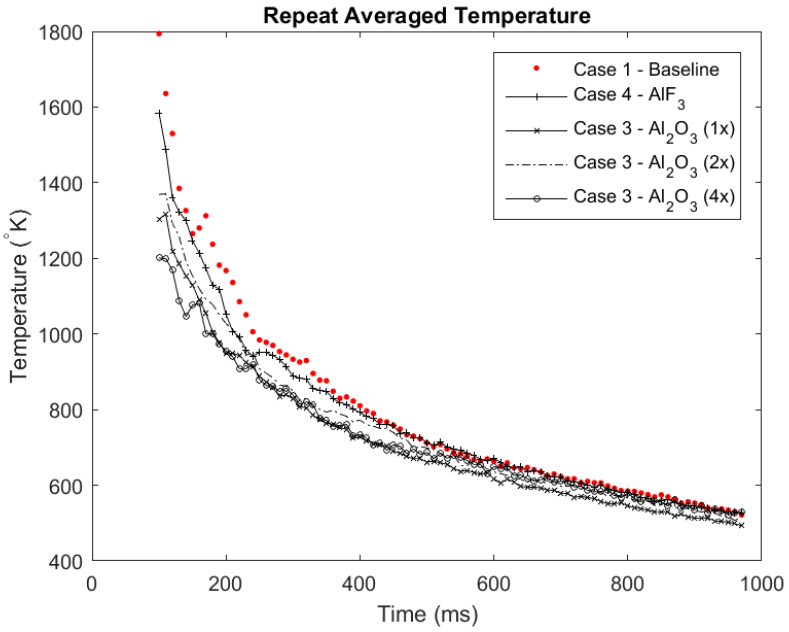

Figure 24: Repeat averaged temperature traces for simplified environment tests

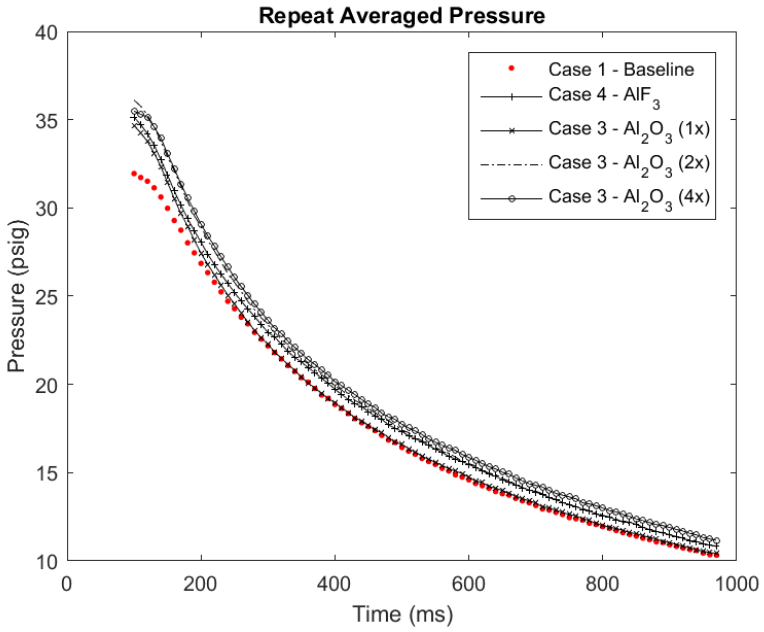

Figure 25: Repeat averaged pressure traces for simplified environment tests

The presence of hydrogen fluoride in the post explosion environment has two important metrics. Similar to the conventional explosives, the impulse, or time-integrated overpressure behind the blast (psi-sec.) is considered to be a measure of effectiveness. Impulse is a function of both magnitude and duration of the positive blast phase. The effectiveness of a C-WMD warhead can be compared to the total exposure of biocidal species, which in the context of this experiment refers to the time-integrated concentration of HF in the chamber.

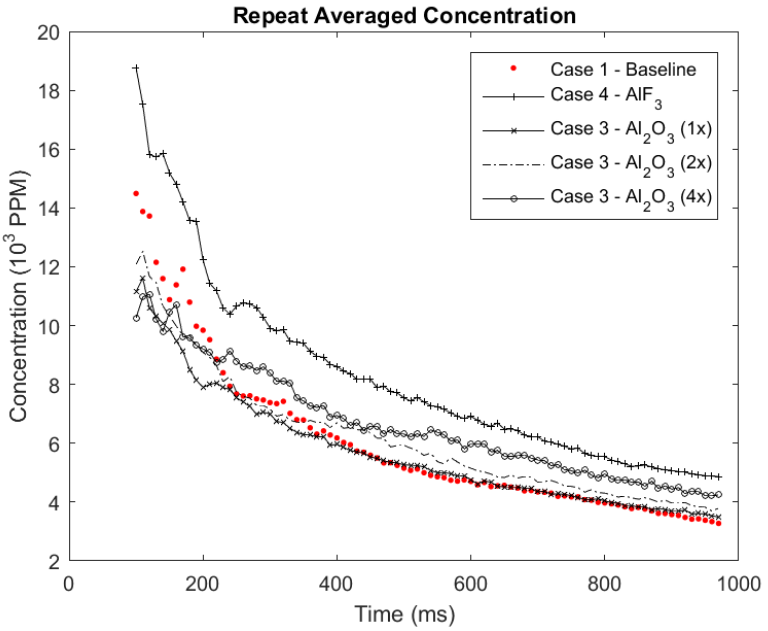

Figure 26: Repeat averaged concentration traces for simplified environment tests

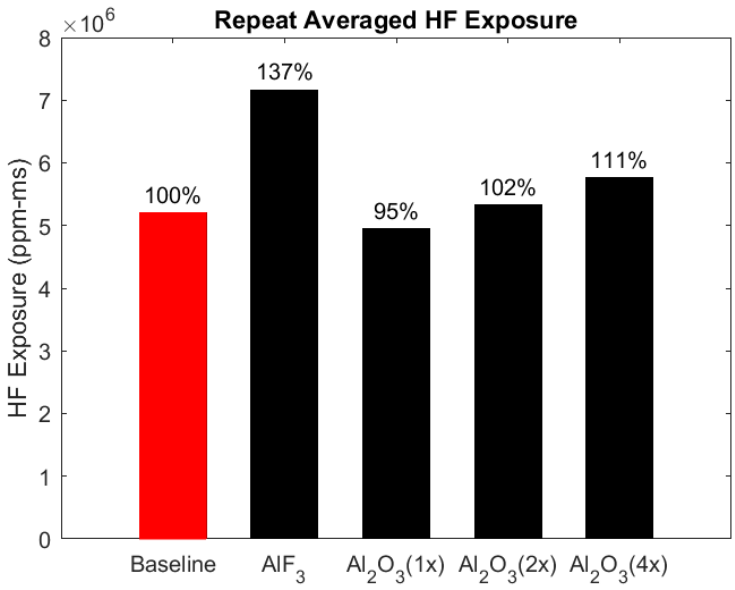

Figure 27: Time integrated, repeat averaged pressure traces for simplified environment tests

The data presented in Figure 26 demonstrated that, on average, there is a slight, but relatively insignificant, sensitivity of HF concentration to the presence of alumina. The discrepancy is more notable at later test times which may be an effect of flame stabilization from the alumina. The observed relationship directly contradicted equilibrium predictions because the presence of higher alumina loadings characteristically slowed the concentration decay relative to our baseline shots. Experiments showed increasing alumina mass resulted in higher concentrations of HF observed particularly at later test times. It is important to see from Figure 24, the gases were on average slightly colder at all of these times as well. It was also shown that explosions with AlF_3 injected had higher temporal and total HF concentrations. This is an important result, because it both verifies the capability of our diagnostics to differentiate hydrogen fluoride yields, as well as it agrees with the equilibrium behavior that at temperatures above 1000 K, AlF_3 will progress towards Al_2O_3 and release its fluorine to contribute supplemental HF. Both

the temporal, and total concentration metrics suggest that we observed this change in our explosions. Since our baseline case contained a linear decay with respect to temperature deviations from that slope were analyzed for the effect of injected powders.

The variability between repeated shots of identical cases is small for the alumina tests. The increase in exposure is notably larger than the deviation between shots, and therefore the positive correlation to mass is credible. The actual percentage relative to the baseline is skewed because baseline tests had a much wider range of exposure values. The non-averaged, time integrated exposures for each test (Test 1 – 18, excluding 15) are shown in Figure 28.

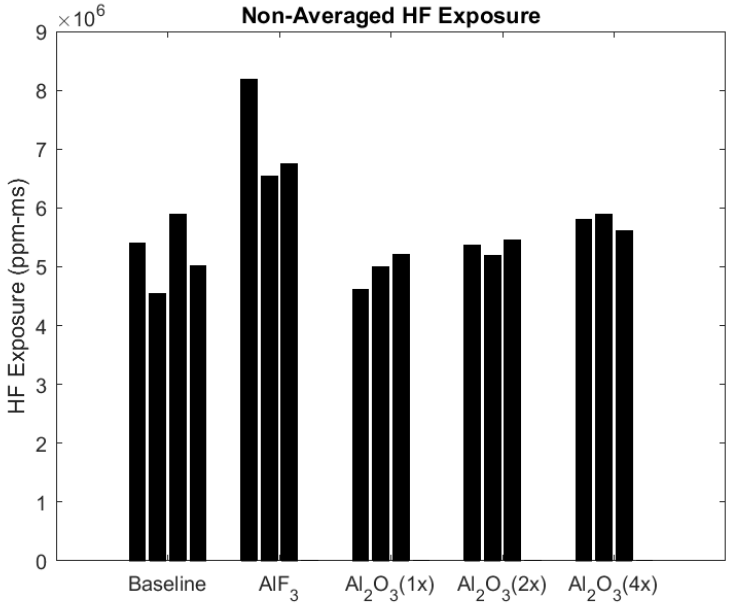

Figure 28: Non - averaged HF exposure

Figure 29 shows the experimentally observed relationship between HF concentration and temperature. These values are directly compared to the equilibrium state predicted when using CHEETAH for a case containing alumina or aluminum. From Figure 4, the degree of suppression

in those two cases is nearly identical. The collected data display incredible linearity between concentration and temperature. In all cases hydrogen fluoride was observed well below temperatures where equilibrium predicts total suppression. There was also no indication of rapid progression toward equilibrium chemistry at any temperature.

In the case of AlF_3 (Case 4), the data showed a notably steeper decay slope. The cases containing Al_2O_3 (Case 3) demonstrated a slightly higher HF concentration at all temperatures with a positive correlation to mass. The slope of concentration decay in alumina cases had a high degree of similarity with respect to each other, as well as the baseline averages. In addition to temporal concentration and total exposure, increasing the mass of alumina also increased the concentration with respect to temperature.

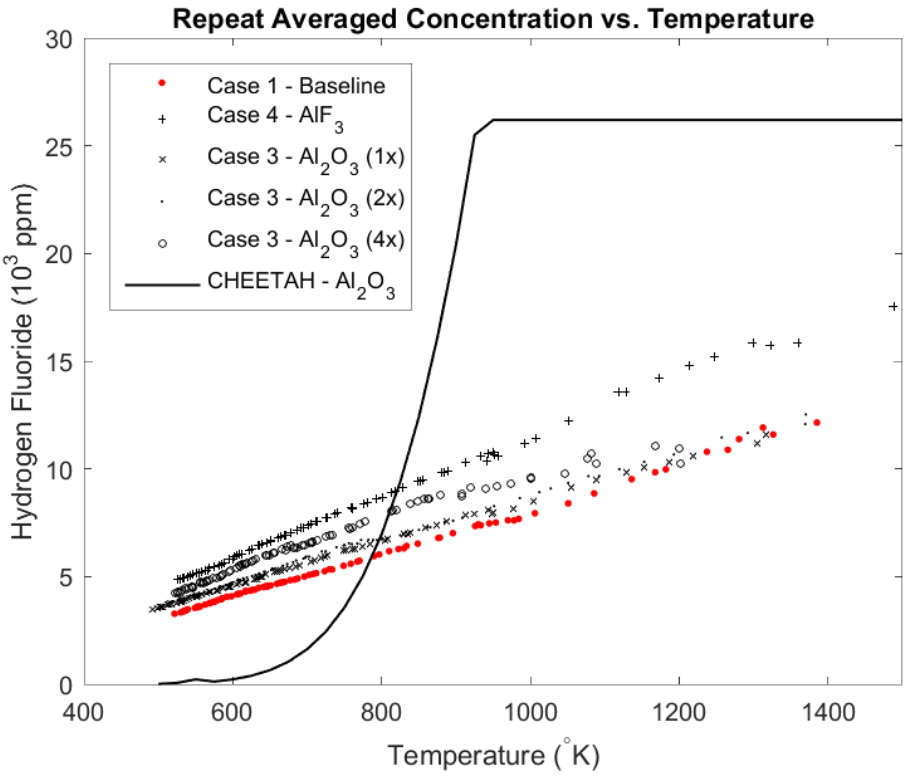

Figure 29: Repeat averaged temperature dependence of concentration

Since this experiment was limited to making measurements after 100 ms, the peak concentrations were not observed. To verify that the DFE achieved full conversion, each data set was linearly fit, and extrapolated back to 2500 K. Figure 30 shows these regressions and provides evidence that in all tests the conversion of the halogen fuel was complete within the accuracy of the experimental method for measuring DFE. This was an important verification, because the deflagration in these explosions was extremely fuel lean, and, to measure any changes in concentration, the initial amount of HF needed to be approximately equal. Even though the regressions appear to suggest there was a measurable difference in initial concentration, this was not the case, as shown by the initial measurements in Figure 26, where the alumina tests actually had lower temporal concentrations on average than the baselines.

Regressions were only used to verify approximate matching between expected and observed conversion given the inherent decay in our concentrations and inability to measure the peak concentration.

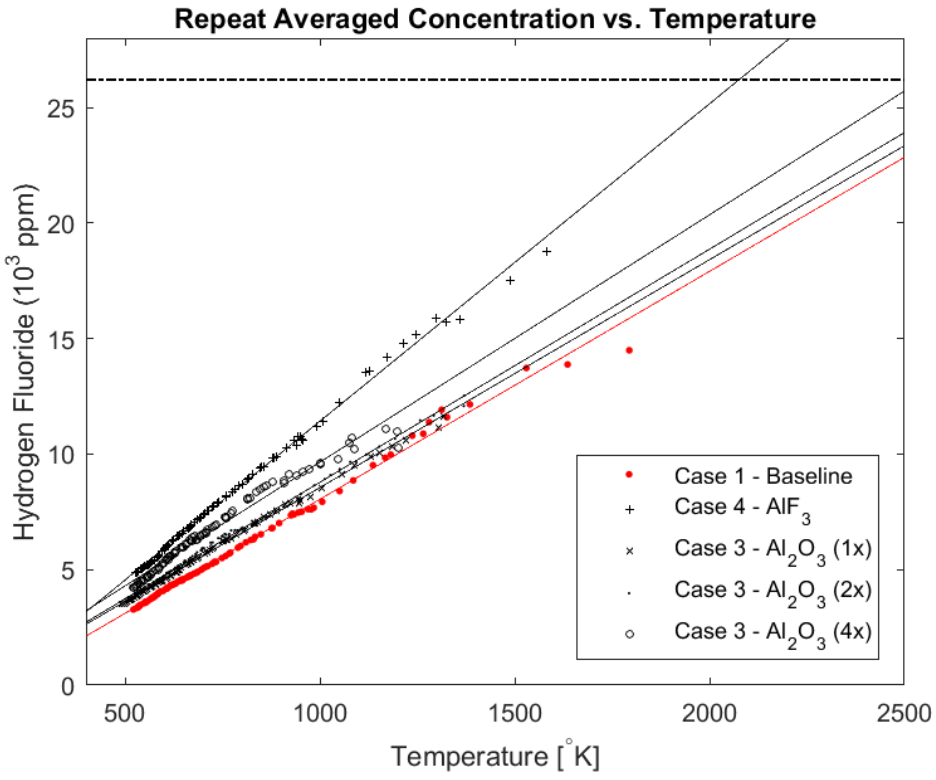

Figure 30: Regression and extrapolation to estimate initial concentrations of HF

The aluminized tests are now presented in comparison to the baselines. Tests with aluminum injection were not averaged, because the pressure traces suggested that each case had a different fraction of aluminum burn, or in a few tests, none at all. From Figure 32, Test 18 and 21 appear to have had aluminum ignition based on the pressure contributions, while Tests 19, 20, and 22 show minimal to no increases. All of the aluminum containing tests are compared to the baseline average (Case 1 – no powder), alumina average (Case 3 – 1x), and aluminum

fluoride average (Case 4 – 1x) in the following results. Both the temperatures and pressures were slightly higher for the duration of the explosion in tests.

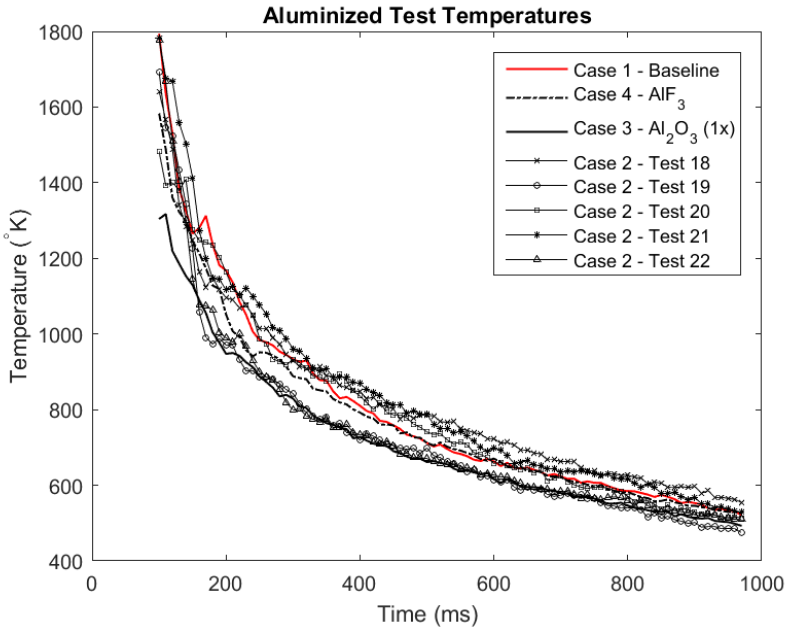

Figure 31: Temperature traces for simplified environment tests with aluminum injection (non-averaged) compared to averaged baseline cases

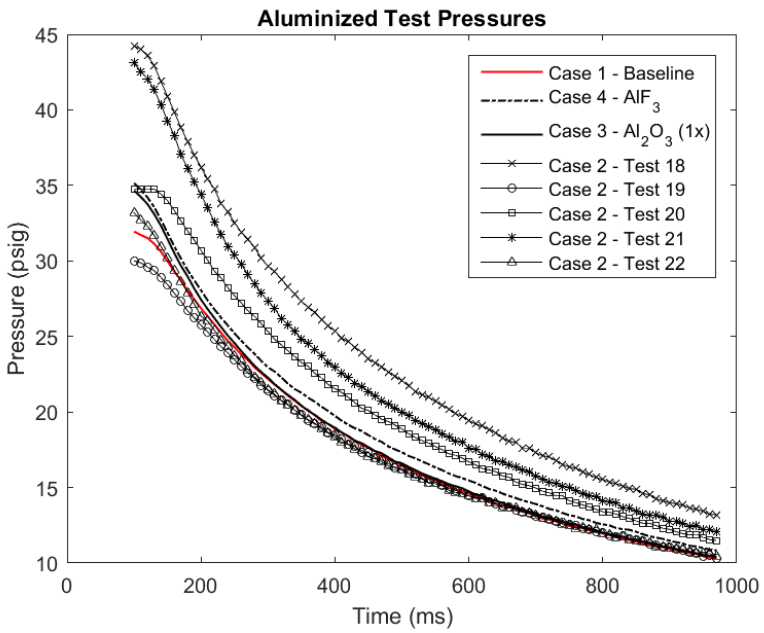

Figure 32: Pressure traces for simplified environment tests with aluminum injection (non-averaged) compared to averaged baseline cases

There temporal curves of aluminized tests in Figure 33 demonstrated very interesting behavior. In Test 18 and 21 where there was significant aluminum combustion, the concentration remained at higher levels for the entire duration of the test. Test 18 even converges to an almost identical level as the averaged baseline for aluminum fluoride. Test 21, which also had a notable pressure increase, demonstrates this same behavior. The cases that did not have characteristics of the aluminum ignition (Tests 19, 20, and 22) match the temporal behavior of the baseline and alumina containing tests to a very high degree.

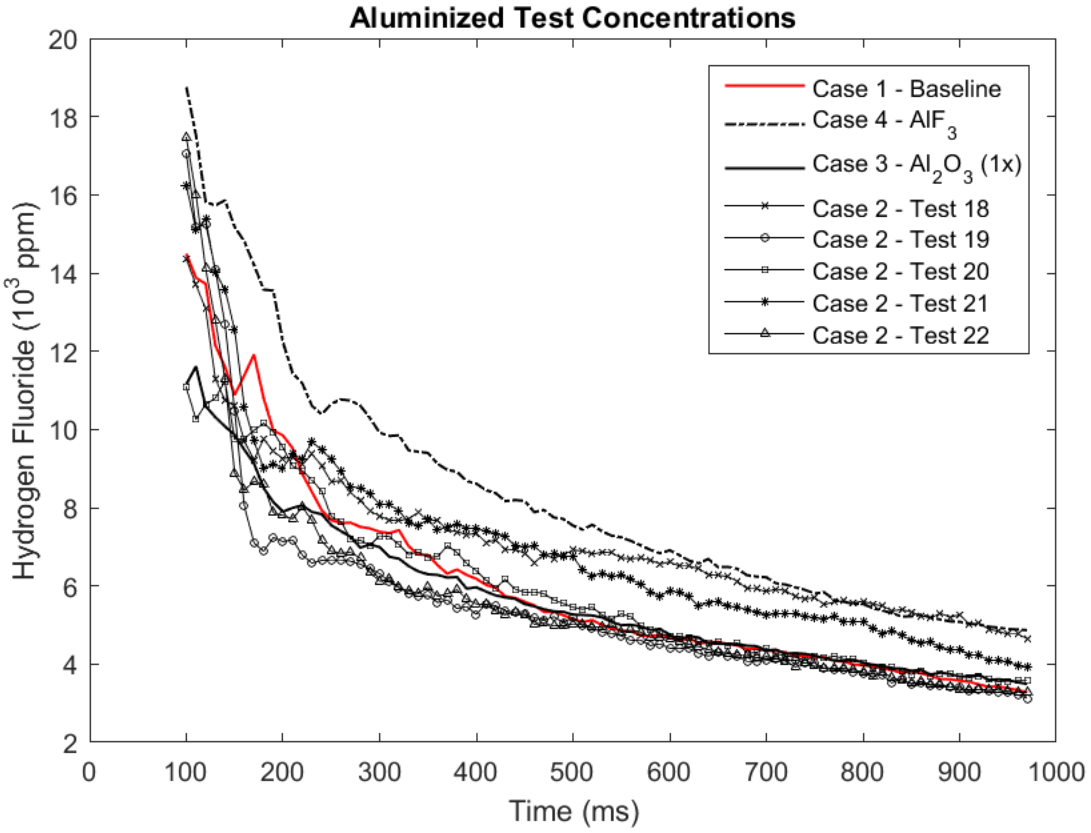

Figure 33: Temporal concentrations of hydrogen fluoride in aluminum injection tests compared to baseline cases

This slight temporal increase in tests 18 and 21 resulted in a significant boost in total exposure, while tests 19, 20, and 22 were conversely diminished. This is a stark difference between aluminum presence and combustion in these explosions. The integrated exposures are presented in Figure 34.

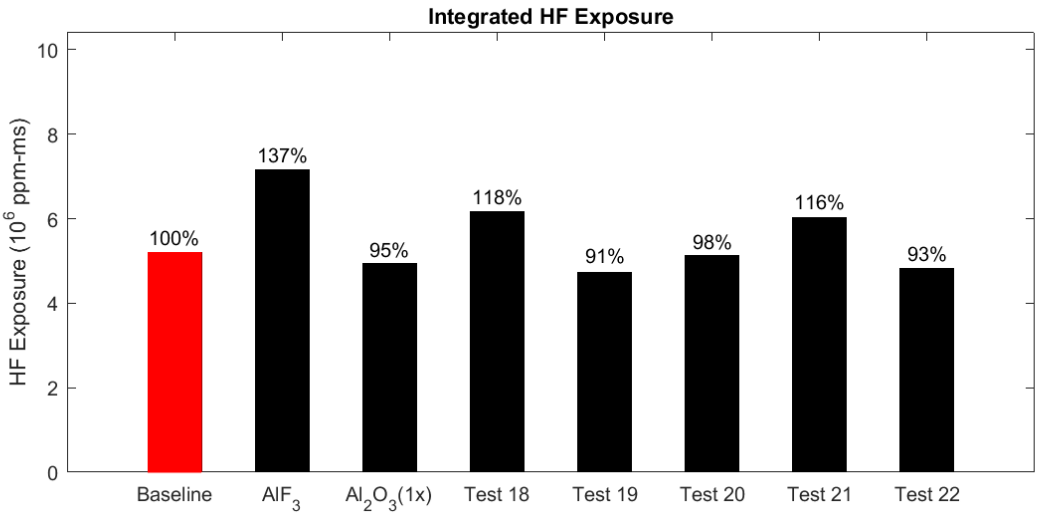

Figure 34: Hydrogen fluoride exposure in aluminum injection tests.

The concentration for the aluminized tests in addition to the regression of case 1, 3 (4x), and 4 averages as a function of temperature is presented in Figure 35. Again, there is evidence of a behavioral difference in the cases where aluminum combustion occurred. The difference is more distinct below 1000 K. This directly contradicts equilibrium predictions.

Tests 18 and 21 appear to be scavenging HF at a faster rate as the gases cool from 800 K to 500 K. This is reflected in their slopes becoming more negative and progressing to baseline level concentrations. This could be an artifact of delayed equilibrium behavior due to the particulate remaining at a higher temperature longer than the surrounding gases from which we are getting our temperature measurement. If the aluminum containing particles remained above the temperature where they are predicted to transform from alumina to aluminum fluoride while surrounding gasses cool, they should not scavenge fluorine away from HF even if kinetics were sufficiently fast.

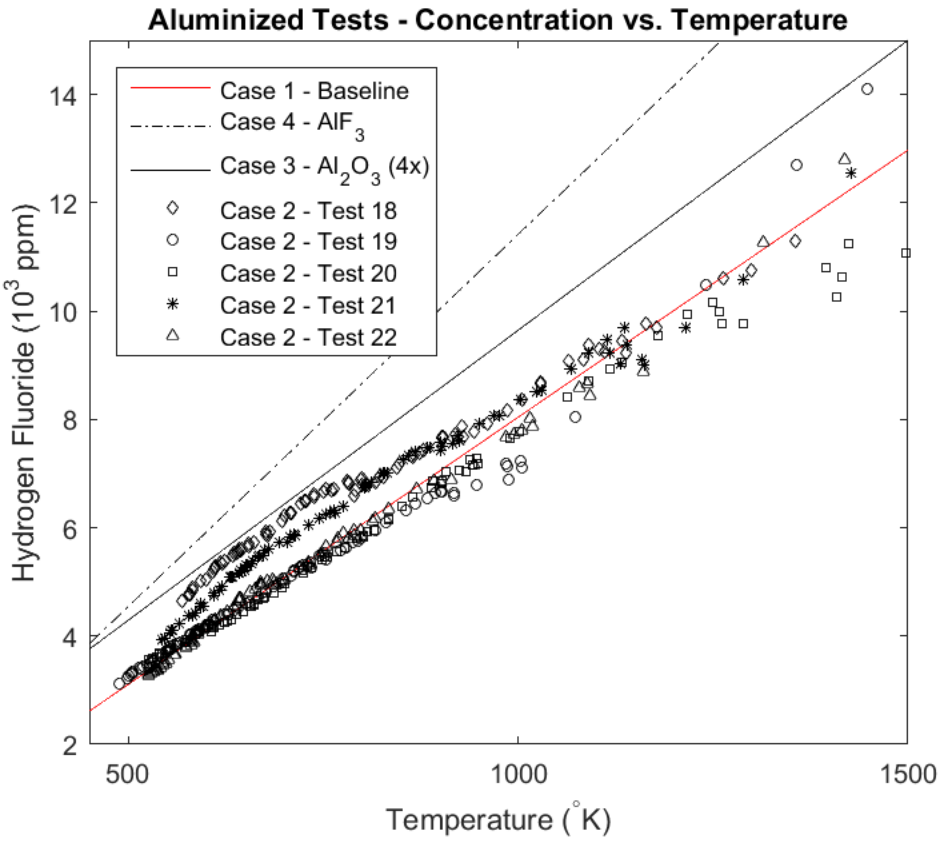

Figure 35: Aluminum injection tests compared to baseline case concentrations versus temperature

A simplified comparison showing a single test of each case is shown in Figure 36. The tests where the aluminum ignited are Test 18 and Test 19. It is very important to see that the concentration of HF is approximately equal to the baseline at higher temperatures, and then transitions over to a curve similar to that of alumina (4x) at approximately 900 K where equilibrium predicts exactly the opposite effect.

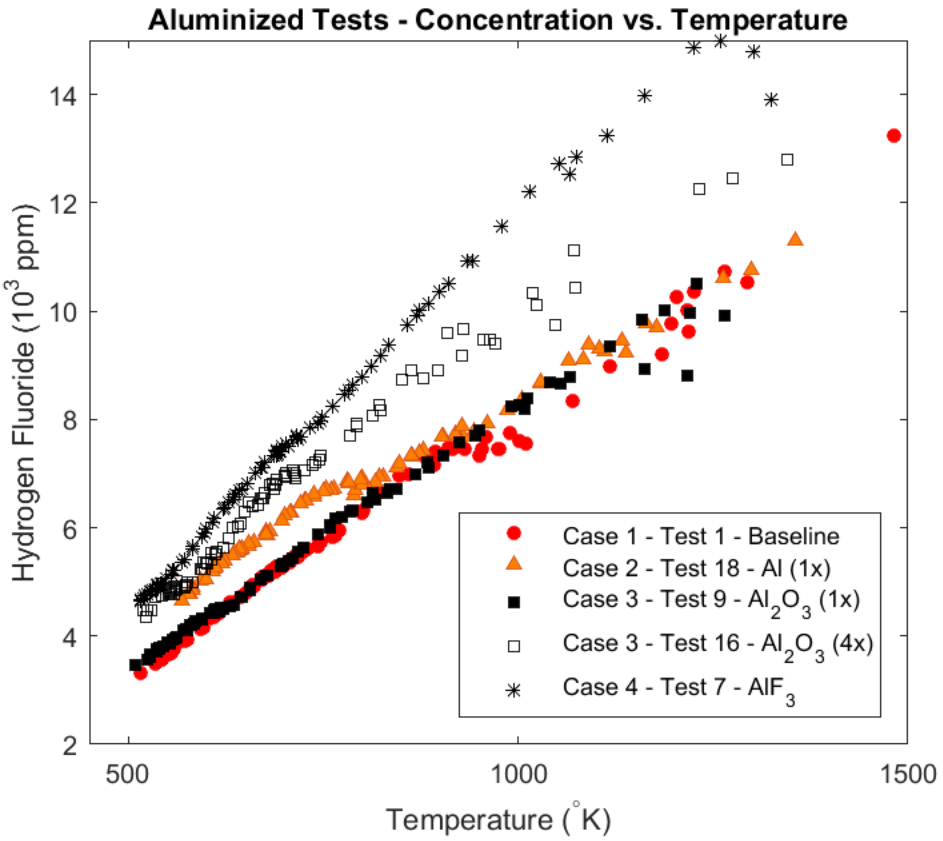

Figure 36: Non-averaged, concentration versus temperature curves for each test case

5.4. Practical Environment Test Results

A total of ten tests were conducted with high explosives to practically replicate the post detonation environment of a C-WMD. As described previously, these tests used RDX and PETN coupled to powdered mixtures of halogen fuels. Similarly to the previous test matrix, the case number refers to the numbered cases simulated in CHEETAH. The multiplier (e.g. 1.5x) refers to the mass of powder additive relative to the 1x required to fully suppress all of the hydrogen fluoride theoretically evolved from full conversion of the halogen fuel. This normalization was also described in Chapter 2, *Equilibrium Simulation and Charge Chemistry Design.* This matrix tested both micro and nano scale alumina powders. Also tested was 3 µm German Flake

aluminum. Test 9 was a Case 1 experiment with PBXN-9 added to raise the temperature of the explosion without adding any aluminum or other materials that could undergo a fluoro-metalic interaction.

The mass of PBXN-9 used was determined by running constant volume explosion simulations in CHEETAH, adding HMX until the predicted temperature was the same as that of the 1x, aluminum case. This number was converted to mass of PBXN-9 taking this polymer bonded explosive to be 92 wt.% HMX. Table 4 presents the test record of practical environment tests involving high explosives.

Table 4: Practical environment test record and masses

Test	Case	PVDF ($C_2H_2F_2$)	PP ($KClO_4$)	Additive		
[#]	[#]	[g]	[g]	[Powder]	[g]	[size μm]
1	1	0.0712	0.0703	-	-	-
2	2 (1x)	0.0680	0.0680	Al (GF)	0.0195	3
3	3 (1x)	0.0747	0.0742	Al_2O_3	0.0393	18-32
4	4 (1x)	0.0718	0.0711	AlF_3	0.0623	-
5	3 (1x)	0.0642	0.0631	Al_2O_3	0.0343	0.3
6	2 (1.5x)	0.0716	0.0698	Al (GF)	0.0309	3
7	3 (1.5x)	0.0679	0.0659	Al_2O_3	0.0528	0.3
8	4 (1.5x)	0.0668	0.0657	AlF_3	0.0871	-
9	1	0.0657	0.0647	PBXN-9	0.1030	-
10*	1 (1.5x)	0.0702	0.0695	Al (GF)	0.0365	0.3

*Baseline test conducted to measure early time HF emission

Temperature and pressure was recorded and calculated in the same fashion as the simplified environment matrix. These tests had lower temporal resolution because a frame rate of 25 ms was used to obtain measurable signal levels on our detector. Quantitative data are presented for time beginning 100 ms after detonation to avoid using optical measurements significantly

convoluted with simultaneous emission. The products of high explosives and our solid state halogen mixtures added substantial mass to the post detonation environment.

The resulting particulate rapidly cooled the explosion by absorbing heat. This is reflected in the temperature curves in Figure 37. In the test conducted with aluminum, the temperature and pressure contributions confirm metal combustion to some degree of completeness. The addition of the PBXN-9 booster raised the pressure to comparable levels as the aluminum. However, it's mass significantly cooled the post detonation flow, since it was five times that of the aluminum added in the "1x" case.

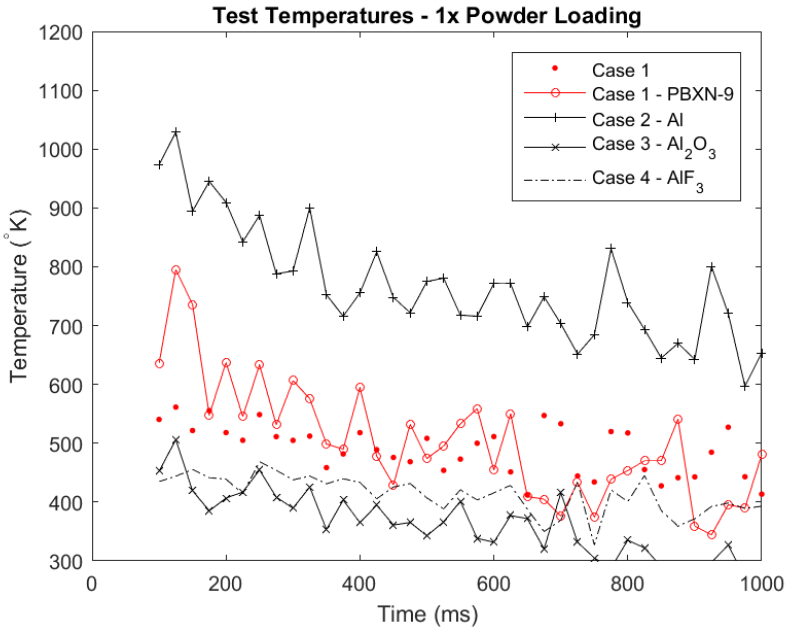

Figure 37: Temperature traces for practical environment tests for the 1x powder loading cases

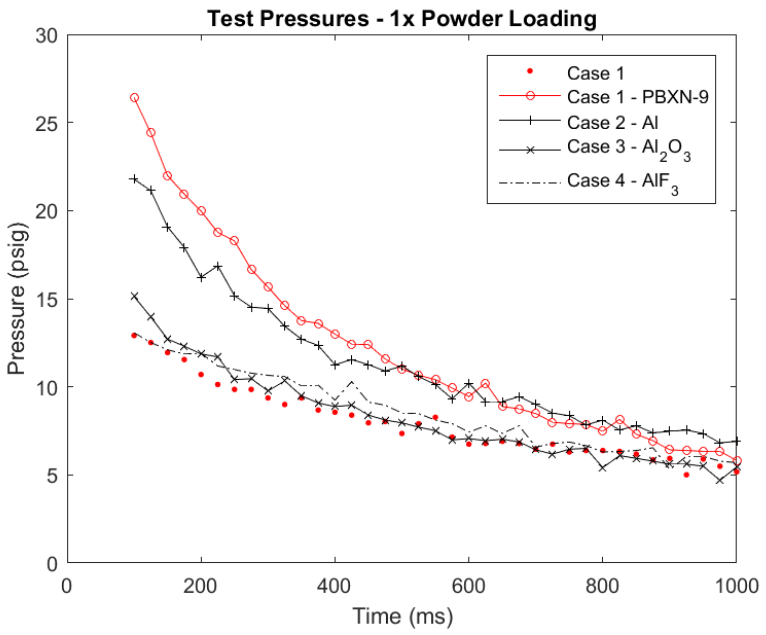

Figure 38: Pressure traces for practical environment tests for the 1x powder loading cases

The resulting data from our tests suggest the breakdown of the halogen fuel may have been incomplete and inconsistent. Additionally, no repeat tests of each case were conducted and therefore no averaging was possible. For this reason, direct comparison of biocidal species concentrations is difficult. The concentration as a function of temperature for both the “1x”, and “1.5x” powder loading is shown below. The total availability of hydrogen fluoride for aluminum to react with is still a factor that potentially affects these data. Therefore partial breakdown of the PVDF does affect the accuracy of each curve.

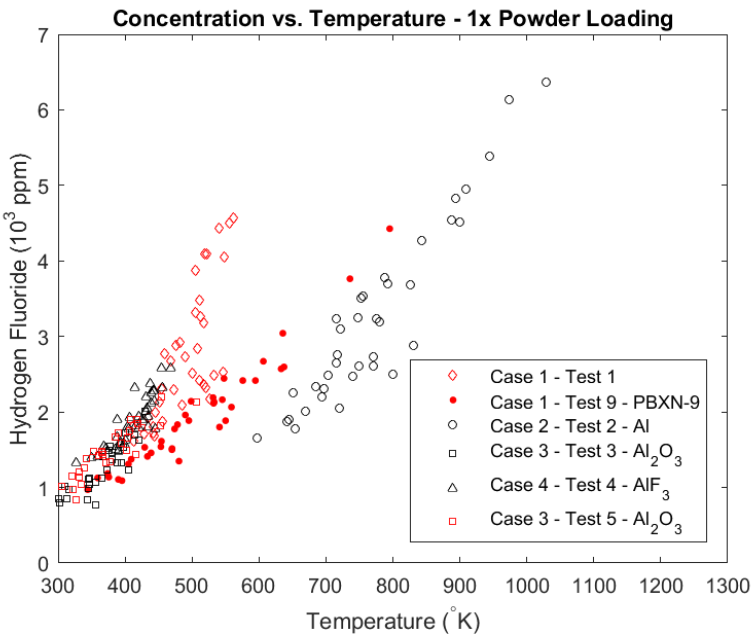

Figure 39: "1x" powder loading concentration versus temperature

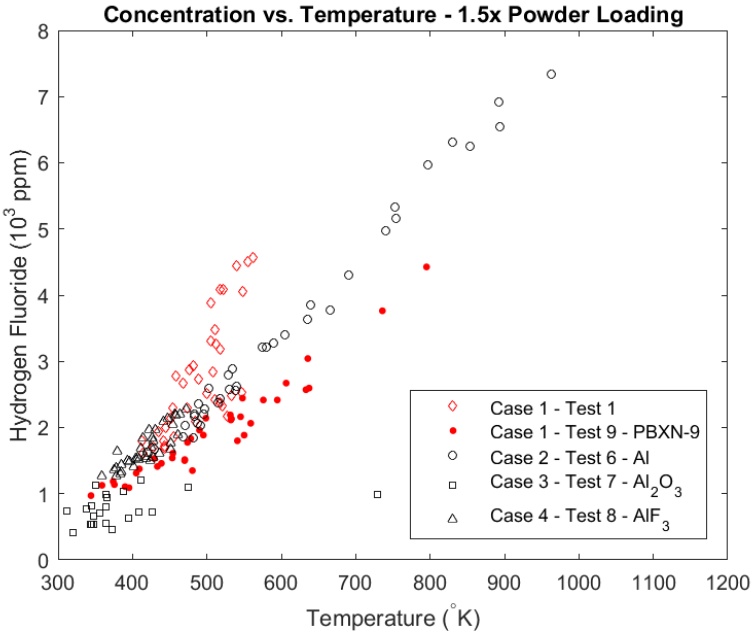

Figure 40: 1.5x powder loading concentration as a function of temperature.

The most important fact in these data is that there were measurable quantities of HF at temperatures significantly below where equilibrium predicts complete suppression. This

statement holds true in all cases where there was aluminum added in any quantity or molecule. These tests also show that in both quantities of powder loading, the aluminized case follows approximately the same trajectory as the alumina, and baseline cases. The 1x case with aluminum does appear to have a steeper slope than the other cases, however this trend did not hold true in the 1.5x test and therefore could be due to a less complete breakdown in the 1x shot. There is not significant evidence to suggest that aluminum is rapidly scavenging fluorine in the first second following these explosions.

5.5. Conclusions

From the data collected in these tests, the first, and most important result is that in both simplified, and practical replications of the C-WMD environment, the presence of biocidal hydrogen fluoride was measured below the temperature that CHEETAH models predict complete suppression. There was no substantial evidence to suggest that the system was progressing toward thermochemical equilibrium within the first second following the explosion.

All tests, including the baseline, showed a linear decay in concentration with respect to temperature. This effect is most likely a chamber wall effect, potentially from the dissociation of HF in the water condensed on surfaces. The immediate next phase of this research is to verify, and quantify this effect so that small shifts toward equilibrium can be differentiated from the other dominating paths for HF removal.

Even though baseline explosions had an unpredicted decay, it is possible to draw conclusions by comparing tests relative to the decay of the baseline case. From the simplified environment

testing, the explosions that contained aluminum combustion had higher HF concentrations than baselines and non-igniting aluminum cases at lower temperatures. This relationship may suggest that the aluminum combustion at the higher temperatures pushes the particles to solid Al_2O_3 and then heat and mass transfer governs composition over chemical kinetics.

The simplified explosions also identified a slight, but positive correlation between mass of alumina injected, and hydrogen fluoride concentration. This is potentially due to flame stabilization from the particles.

The simplified environment testing with AlF_3 also demonstrated that the release of fluorine was rapid, and the recovery was sufficiently slow, or that aluminum atoms became trapped as alumina at higher temperatures. As an additive to the explosion, aluminum fluoride provided a significant boost in concentration of biocidal HF with respect to both time, and temperature. This could have potential application as an RM in C-WMD platforms as an efficient package of fluorine atoms.

5.6. Future Work

Future work will need to identify why the baseline experiments demonstrated a decrease in HF concentration, when models suggest there should not be any. As mentioned earlier, one possibility is that the HF is dissociating in condensed water on the chamber walls. This would remove gas phase HF population such as what was observed. In order to address the issue of temperature inhomogeneity between the chamber walls and gas species, a computational analysis should be conducted to model the chamber wall interaction including phase change. It

may be beneficial to run experiments with a chamber liner of less reactive, or different density material, such as fused silica to mitigate the heat transfer effects. Another valuable test to address heat transfer and condensation would be to preheat the chamber prior to the explosion, or alter the surface area of wall.

An alternative method to address the condensation-driven removal of HF is to vary the reactant chemistry to remove water from the products. These tests used propane as a non-halogenated reactant, but the side effect of this was it resulted in significant amounts of water in the chamber after combustion. Shortening the absorption path length to preserve spectral line sensitivity, and burning only reactants with a 1:1, H:F ratio such as difluoromethane will result in reduced water in the products.

If the anhydrous baseline explosion still exhibits the same decay, then the aluminum chamber wall may be inducing a reaction on its own. This is a difficult challenge to address because HF is so reactive with most metals, however a high density poly-ethylene (HDPE) liner may be sufficiently inert, providing it does not decompose during the explosion.

The work presented here suggests that the kinetics are sufficiently slow at certain key conditions, but also lays excellent ground work for the development of a complete combustion model for the aluminum particles in the presence hydrogen fluoride.

The addition of a post-explosion residue analysis using energy dispersion spectroscopy (EDS) to look for fluorine atoms on the surface of particles in the explosion would be potentially insightful for defining a combustion mechanism in fluorine rich environment. This would go

hand in hand with an X-ray diffraction analysis to look at the molecular composition of the particles. From this, one would obtain a mass fraction of residue that was AlF_3 versus that of Al_2O_3, and from the EDS we could verify that the fluorination is taking place on the surface. The most important case to analyze might be to inject AlF_3, and then see if the recovered powder is Al_2O_3.

There is also a need to test the dependence of HF availability on the rate of formation of aluminum fluoride. Based on the long path length of the chamber used, we were limited in our study to making measurements in less than 3% mole fraction, so that our absorption depths remained roughly linearly dependent on concentration. A simple modification to the chamber to accommodate a shorter path length would enable the same test matrix to be run at higher concentrations so the aluminum has more HF to interact with. In the context of the simplified environment, signal transmission was not at all a limitation, so much weaker absorptions would be quantifiable, and therefore a shorter path length can be used.

Lastly, substantial work went into developing the diagnostic for quantitative, high speed, infrared spectroscopic measurements of HF. Now that there is a proven method for measuring the precise HF yield in optically thick explosions, a panel of tests should be conducted on state of the art HF producing RM's. This matrix could compare the HF production between HFNX, thermites, and any other proposed RM's on a per unit mass basis. With that information, the military would be able to select the most efficient way to deliver HF to the target.

REFERENCES

[1] D. L. Goldfein, "Countering Weapons of Mass Destruction, JP 3-40," Chairman of the Joint Chiefs of Staff (CJCS), 2014.

[2] Defense Threat Reduction Agency, "Thrust Area 4 - Science to Defeat WMD," [Online]. Available: http://www.dtra.mil/Research/BasicandAppliedScienceDepartment/SciencetoDefeatWMD.aspx. [Accessed 27 March 2016].

[3] R. D. Chapman, "N,N-Dihaloamine Explosives as Harmful Agent Defeat Materials, MIPR 10-2953," Defense Threat Reduction Agency, Fort Belevoir, 2014.

[4] J. Feng, G. Jian, Q. Liu and M. R. Zachariah, "Passivated Iodine Pentoxide Oxidizer for Potential Biocidal Nanoenergetic Applications," *ACS Applied Materials & Interfaces,* vol. 5, no. 18, p. 8875–8880, 2013.

[5] D. J. Allen, M.S. Thesis, Optical Combustion Measurments of Novel Energetic Materials in a Heterogenous Shock Tube, Urbana-Champaign: University of Illinois, Mechanical Science and Engineering Department, 2012.

[6] M. D. Clemenson, M.S.Thesis, Explosive Initiation of the Various Forms of the Ti/2B Energetic System, Urbana-Champaign: University of Illinois, Mechanical Science and Engineering Department, 2012.

[7] J. Henderson, A. W. Longbottom, A. M. Milne, J. M. Lightstone, C. Milby, D. Stamatis, F. R. Svingala, A. L. Daniels, M. Bensman, M. Bohmke and K. Miller, "Experiments and Modeling for Biocidal Effects of Explosives," *Propellants, Explosives, Pyrotechnics,* vol. 35, pp. 1-9, 2010.

[8] K. C. Gottiparthi, J. C. Schulz and S. Menon, "On the Neutralization of Bacterial Spores in Post-detonation Flows," *Shock Waves,* vol. 24, pp. 455-466, 2014.

[9] "RP-80 EBW Detonator," Teledyne RISI, 2011. [Online]. Available: http://www.teledynerisi.com/products/0products_1ebw_page23.asp. [Accessed 2016].

[10] D. L. S. Rothman, "The HITRAN Database," Atomic and Molecular Physics Division, Harvard-Smithsonian Center for Astrophysics, [Online]. Available: http://hitran.org.

[11] N. M. Laurendeau, Statistical Thermodynamics: Fundamentals and Applications, New York, New York: Cambridge University Press, 2005.

[12] R. K. Hanson, R. M. Spearrin and C. S. Goldenstein, Spectroscopy and Optical Diagnostics for Gases, New York: Springer, 2016.

[13] S.-I. Chou, D. S. Baer and R. K. Hanson, "Diode–Laser Measurements of He-, Ar-, and N2-Broadened HF Lineshapes in the First Overtone Band," *Journal of Molecular Spectroscopy,* vol. 196, pp. 70-76, 1999.

[14] K. P. Huber and G. Herzberg, "NIST Chemistry WebBook," National Institute for Standards a, [Online]. Available: http://webbook.nist.gov/cgi/cbook.cgi?ID=C7664393&Mask=1000#Diatomic.

[15] D. L. Goldfein, "Operations is Chemical, Biological, Radiological, and Nuclear Environments, JP 3-11," Chairment of the Joint Chiefs of Staff, 2013.